

Evidence for the $B^0 \rightarrow p\bar{p}K^{*0}$ and $B^+ \rightarrow \eta_c K^{*+}$ decays and Study of the Decay Dynamics of B Meson Decays into $p\bar{p}h$ Final States.

B. Aubert,¹ M. Bona,¹ D. Boutigny,¹ Y. Karyotakis,¹ J. P. Lees,¹ V. Poireau,¹ X. Prudent,¹ V. Tisserand,¹ A. Zghiche,¹ J. Garra Tico,² E. Grauges,² L. Lopez,³ A. Palano,³ G. Eigen,⁴ B. Stugu,⁴ L. Sun,⁴ G. S. Abrams,⁵ M. Battaglia,⁵ D. N. Brown,⁵ J. Button-Shafer,⁵ R. N. Cahn,⁵ Y. Groysman,⁵ R. G. Jacobsen,⁵ J. A. Kadyk,⁵ L. T. Kerth,⁵ Yu. G. Kolomensky,⁵ G. Kukartsev,⁵ D. Lopes Pegna,⁵ G. Lynch,⁵ L. M. Mir,⁵ T. J. Orimoto,⁵ M. T. Ronan,^{5,*} K. Tackmann,⁵ W. A. Wenzel,⁵ P. del Amo Sanchez,⁶ C. M. Hawkes,⁶ N. Soni,⁶ A. T. Watson,⁶ T. Held,⁷ H. Koch,⁷ B. Lewandowski,⁷ M. Pelizaeus,⁷ T. Schroeder,⁷ M. Steinke,⁷ D. Walker,⁸ D. J. Asgeirsson,⁹ T. Cuhadar-Donszelmann,⁹ B. G. Fulsom,⁹ C. Hearty,⁹ T. S. Mattison,⁹ J. A. McKenna,⁹ A. Khan,¹⁰ M. Saleem,¹⁰ L. Teodorescu,¹⁰ V. E. Blinov,¹¹ A. D. Bukin,¹¹ V. P. Druzhinin,¹¹ V. B. Golubev,¹¹ A. P. Onuchin,¹¹ S. I. Serednyakov,¹¹ Yu. I. Skovpen,¹¹ E. P. Solodov,¹¹ K. Yu. Todyshev,¹¹ M. Bondioli,¹² S. Curry,¹² I. Eschrich,¹² D. Kirkby,¹² A. J. Lankford,¹² P. Lund,¹² M. Mandelkern,¹² E. C. Martin,¹² D. P. Stoker,¹² S. Abachi,¹³ C. Buchanan,¹³ S. D. Foulkes,¹⁴ J. W. Gary,¹⁴ F. Liu,¹⁴ O. Long,¹⁴ B. C. Shen,¹⁴ L. Zhang,¹⁴ H. P. Paar,¹⁵ S. Rahatlou,¹⁵ V. Sharma,¹⁵ J. W. Berryhill,¹⁶ C. Campagnari,¹⁶ A. Cunha,¹⁶ B. Dahmes,¹⁶ T. M. Hong,¹⁶ D. Kovalskiy,¹⁶ J. D. Richman,¹⁶ T. W. Beck,¹⁷ A. M. Eisner,¹⁷ C. J. Flacco,¹⁷ C. A. Heusch,¹⁷ J. Kroseberg,¹⁷ W. S. Lockman,¹⁷ T. Schalk,¹⁷ B. A. Schumm,¹⁷ A. Seiden,¹⁷ M. G. Wilson,¹⁷ L. O. Winstrom,¹⁷ E. Chen,¹⁸ C. H. Cheng,¹⁸ F. Fang,¹⁸ D. G. Hitlin,¹⁸ I. Narsky,¹⁸ T. Piatenko,¹⁸ F. C. Porter,¹⁸ R. Andreassen,¹⁹ G. Mancinelli,¹⁹ B. T. Meadows,¹⁹ K. Mishra,¹⁹ M. D. Sokoloff,¹⁹ F. Blanc,²⁰ P. C. Bloom,²⁰ S. Chen,²⁰ W. T. Ford,²⁰ J. F. Hirschauer,²⁰ A. Kreisel,²⁰ M. Nagel,²⁰ U. Nauenberg,²⁰ A. Olivas,²⁰ J. G. Smith,²⁰ K. A. Ulmer,²⁰ S. R. Wagner,²⁰ J. Zhang,²⁰ A. M. Gabareen,²¹ A. Soffer,²¹ W. H. Toki,²¹ R. J. Wilson,²¹ F. Winklmeier,²¹ D. D. Altenburg,²² E. Feltresi,²² A. Hauke,²² H. Jasper,²² J. Merkel,²² A. Petzold,²² B. Spaan,²² K. Wacker,²² V. Klose,²³ M. J. Kobel,²³ H. M. Lacker,²³ W. F. Mader,²³ R. Nogowski,²³ J. Schubert,²³ K. R. Schubert,²³ R. Schwierz,²³ J. E. Sundermann,²³ A. Volk,²³ D. Bernard,²⁴ G. R. Bonneaud,²⁴ E. Latour,²⁴ V. Lombardo,²⁴ Ch. Thiebaut,²⁴ M. Verderi,²⁴ P. J. Clark,²⁵ W. Gradl,²⁵ F. Muheim,²⁵ S. Playfer,²⁵ A. I. Robertson,²⁵ Y. Xie,²⁵ M. Andreotti,²⁶ D. Bettoni,²⁶ C. Bozzi,²⁶ R. Calabrese,²⁶ A. Cecchi,²⁶ G. Cibinetto,²⁶ P. Franchini,²⁶ E. Luppi,²⁶ M. Negrini,²⁶ A. Petrella,²⁶ L. Piemontese,²⁶ E. Prencipe,²⁶ V. Santoro,²⁶ F. Anulli,²⁷ R. Baldini-Ferroli,²⁷ A. Calcaterra,²⁷ R. de Sangro,²⁷ G. Finocchiaro,²⁷ S. Pacetti,²⁷ P. Patteri,²⁷ I. M. Peruzzi,^{27, †} M. Piccolo,²⁷ M. Rama,²⁷ A. Zallo,²⁷ A. Buzzo,²⁸ R. Contri,²⁸ M. Lo Vetere,²⁸ M. M. Macri,²⁸ M. R. Monge,²⁸ S. Passaggio,²⁸ C. Patrignani,²⁸ E. Robutti,²⁸ A. Santroni,²⁸ S. Tosi,²⁸ K. S. Chaisanguanthum,²⁹ M. Morii,²⁹ J. Wu,²⁹ R. S. Dubitzky,³⁰ J. Marks,³⁰ S. Schenk,³⁰ U. Uwer,³⁰ D. J. Bard,³¹ P. D. Dauncey,³¹ R. L. Flack,³¹ J. A. Nash,³¹ W. Panduro Vazquez,³¹ M. Tibbetts,³¹ P. K. Behera,³² X. Chai,³² M. J. Charles,³² U. Mallik,³² V. Ziegler,³² J. Cochran,³³ H. B. Crawley,³³ L. Dong,³³ V. Eyges,³³ W. T. Meyer,³³ S. Prell,³³ E. I. Rosenberg,³³ A. E. Rubin,³³ Y. Y. Gao,³⁴ A. V. Gritsan,³⁴ Z. J. Guo,³⁴ C. K. Lae,³⁴ A. G. Denig,³⁵ M. Fritsch,³⁵ G. Schott,³⁵ N. Arnaud,³⁶ J. Béquilleux,³⁶ M. Davier,³⁶ G. Grosdidier,³⁶ A. Höcker,³⁶ V. Lepeltier,³⁶ F. Le Diberder,³⁶ A. M. Lutz,³⁶ S. Pruvot,³⁶ S. Rodier,³⁶ P. Roudeau,³⁶ M. H. Schune,³⁶ J. Serrano,³⁶ V. Sordini,³⁶ A. Stocchi,³⁶ W. F. Wang,³⁶ G. Wormser,³⁶ D. J. Lange,³⁷ D. M. Wright,³⁷ I. Bingham,³⁸ C. A. Chavez,³⁸ I. J. Forster,³⁸ J. R. Fry,³⁸ E. Gabathuler,³⁸ R. Gamet,³⁸ D. E. Hutchcroft,³⁸ D. J. Payne,³⁸ K. C. Schofield,³⁸ C. Touramanis,³⁸ A. J. Bevan,³⁹ K. A. George,³⁹ F. Di Lodovico,³⁹ W. Menges,³⁹ R. Sacco,³⁹ G. Cowan,⁴⁰ H. U. Flaecher,⁴⁰ D. A. Hopkins,⁴⁰ S. Paramesvaran,⁴⁰ F. Salvatore,⁴⁰ A. C. Wren,⁴⁰ D. N. Brown,⁴¹ C. L. Davis,⁴¹ J. Allison,⁴² N. R. Barlow,⁴² R. J. Barlow,⁴² Y. M. Chia,⁴² C. L. Edgar,⁴² G. D. Lafferty,⁴² T. J. West,⁴² J. I. Yi,⁴² J. Anderson,⁴³ C. Chen,⁴³ A. Jawahery,⁴³ D. A. Roberts,⁴³ G. Simi,⁴³ J. M. Tuggle,⁴³ G. Blaylock,⁴⁴ C. Dallapiccola,⁴⁴ S. S. Hertzbach,⁴⁴ X. Li,⁴⁴ T. B. Moore,⁴⁴ E. Salvati,⁴⁴ S. Saremi,⁴⁴ R. Cowan,⁴⁵ D. Dujmic,⁴⁵ P. H. Fisher,⁴⁵ K. Koeneke,⁴⁵ G. Sciolla,⁴⁵ S. J. Sekula,⁴⁵ M. Spitznagel,⁴⁵ F. Taylor,⁴⁵ R. K. Yamamoto,⁴⁵ M. Zhao,⁴⁵ Y. Zheng,⁴⁵ S. E. Mclachlin,^{46,*} P. M. Patel,⁴⁶ S. H. Robertson,⁴⁶ A. Lazzaro,⁴⁷ F. Palombo,⁴⁷ J. M. Bauer,⁴⁸ L. Cremaldi,⁴⁸ V. Eschenburg,⁴⁸ R. Godang,⁴⁸ R. Kroeger,⁴⁸ D. A. Sanders,⁴⁸ D. J. Summers,⁴⁸ H. W. Zhao,⁴⁸ S. Brunet,⁴⁹ D. Côté,⁴⁹ M. Simard,⁴⁹ P. Taras,⁴⁹ F. B. Viaud,⁴⁹ H. Nicholson,⁵⁰ G. De Nardo,⁵¹ F. Fabozzi,^{51, ‡} L. Lista,⁵¹ D. Monorchio,⁵¹ C. Sciacca,⁵¹ M. A. Baak,⁵² G. Raven,⁵² H. L. Snoek,⁵² C. P. Jessop,⁵³ J. M. LoSecco,⁵³ G. Benelli,⁵⁴ L. A. Corwin,⁵⁴

K. Honscheid,⁵⁴ H. Kagan,⁵⁴ R. Kass,⁵⁴ J. P. Morris,⁵⁴ A. M. Rahimi,⁵⁴ J. J. Regensburger,⁵⁴ Q. K. Wong,⁵⁴
 N. L. Blount,⁵⁵ J. Brau,⁵⁵ R. Frey,⁵⁵ O. Igonkina,⁵⁵ J. A. Kolb,⁵⁵ M. Lu,⁵⁵ R. Rahmat,⁵⁵ N. B. Sinev,⁵⁵
 D. Strom,⁵⁵ J. Strube,⁵⁵ E. Torrence,⁵⁵ N. Gagliardi,⁵⁶ A. Gaz,⁵⁶ M. Margoni,⁵⁶ M. Morandin,⁵⁶ A. Pompili,⁵⁶
 M. Posocco,⁵⁶ M. Rotondo,⁵⁶ F. Simonetto,⁵⁶ R. Stroili,⁵⁶ C. Voci,⁵⁶ E. Ben-Haim,⁵⁷ H. Briand,⁵⁷ G. Calderini,⁵⁷
 J. Chauveau,⁵⁷ P. David,⁵⁷ L. Del Buono,⁵⁷ Ch. de la Vaissière,⁵⁷ O. Hamon,⁵⁷ Ph. Leruste,⁵⁷ J. Malclès,⁵⁷
 J. Ocariz,⁵⁷ A. Perez,⁵⁷ L. Gladney,⁵⁸ M. Biasini,⁵⁹ R. Covarelli,⁵⁹ E. Manoni,⁵⁹ C. Angelini,⁶⁰ G. Batignani,⁶⁰
 S. Bettarini,⁶⁰ M. Carpinelli,⁶⁰ R. Cenci,⁶⁰ A. Cervelli,⁶⁰ F. Forti,⁶⁰ M. A. Giorgi,⁶⁰ A. Lusiani,⁶⁰ G. Marchiori,⁶⁰
 M. A. Mazur,⁶⁰ M. Morganti,⁶⁰ N. Neri,⁶⁰ E. Paoloni,⁶⁰ G. Rizzo,⁶⁰ J. J. Walsh,⁶⁰ M. Haire,⁶¹ J. Biesiada,⁶²
 P. Elmer,⁶² Y. P. Lau,⁶² C. Lu,⁶² J. Olsen,⁶² A. J. S. Smith,⁶² A. V. Telnov,⁶² E. Baracchini,⁶³ F. Bellini,⁶³
 G. Cavoto,⁶³ A. D’Orazio,⁶³ D. del Re,⁶³ E. Di Marco,⁶³ R. Faccini,⁶³ F. Ferrarotto,⁶³ F. Ferroni,⁶³ M. Gaspero,⁶³
 P. D. Jackson,⁶³ L. Li Gioi,⁶³ M. A. Mazzoni,⁶³ S. Morganti,⁶³ G. Piredda,⁶³ F. Polci,⁶³ F. Renga,⁶³ C. Voena,⁶³
 M. Ebert,⁶⁴ T. Hartmann,⁶⁴ H. Schröder,⁶⁴ R. Waldi,⁶⁴ T. Adye,⁶⁵ G. Castelli,⁶⁵ B. Franek,⁶⁵ E. O. Olaiya,⁶⁵
 S. Ricciardi,⁶⁵ W. Roethel,⁶⁵ F. F. Wilson,⁶⁵ R. Aleksan,⁶⁶ S. Emery,⁶⁶ M. Escalier,⁶⁶ A. Gaidot,⁶⁶ S. F. Ganzhur,⁶⁶
 G. Hamel de Monchenault,⁶⁶ W. Kozanecki,⁶⁶ G. Vasseur,⁶⁶ Ch. Yèche,⁶⁶ M. Zito,⁶⁶ X. R. Chen,⁶⁷ H. Liu,⁶⁷
 W. Park,⁶⁷ M. V. Purohit,⁶⁷ J. R. Wilson,⁶⁷ M. T. Allen,⁶⁸ D. Aston,⁶⁸ R. Bartoldus,⁶⁸ P. Bechtle,⁶⁸ N. Berger,⁶⁸
 R. Claus,⁶⁸ J. P. Coleman,⁶⁸ M. R. Convery,⁶⁸ J. C. Dingfelder,⁶⁸ J. Dorfan,⁶⁸ G. P. Dubois-Felsmann,⁶⁸
 W. Dunwoodie,⁶⁸ R. C. Field,⁶⁸ T. Glanzman,⁶⁸ S. J. Gowdy,⁶⁸ M. T. Graham,⁶⁸ P. Grenier,⁶⁸ C. Hast,⁶⁸
 T. Hryn’ova,⁶⁸ W. R. Innes,⁶⁸ J. Kaminski,⁶⁸ M. H. Kelsey,⁶⁸ H. Kim,⁶⁸ P. Kim,⁶⁸ M. L. Kocian,⁶⁸
 D. W. G. S. Leith,⁶⁸ S. Li,⁶⁸ S. Luitz,⁶⁸ V. Luth,⁶⁸ H. L. Lynch,⁶⁸ D. B. MacFarlane,⁶⁸ H. Marsiske,⁶⁸ R. Messner,⁶⁸
 D. R. Muller,⁶⁸ C. P. O’Grady,⁶⁸ I. Ofte,⁶⁸ A. Perazzo,⁶⁸ M. Perl,⁶⁸ T. Pulliam,⁶⁸ B. N. Ratcliff,⁶⁸
 A. Roodman,⁶⁸ A. A. Salnikov,⁶⁸ R. H. Schindler,⁶⁸ J. Schwiening,⁶⁸ A. Snyder,⁶⁸ J. Stelzer,⁶⁸ D. Su,⁶⁸
 M. K. Sullivan,⁶⁸ K. Suzuki,⁶⁸ S. K. Swain,⁶⁸ J. M. Thompson,⁶⁸ J. Va’vra,⁶⁸ N. van Bakel,⁶⁸ A. P. Wagner,⁶⁸
 M. Weaver,⁶⁸ W. J. Wisniewski,⁶⁸ M. Wittgen,⁶⁸ D. H. Wright,⁶⁸ A. K. Yarritu,⁶⁸ K. Yi,⁶⁸ C. C. Young,⁶⁸
 P. R. Burchat,⁶⁹ A. J. Edwards,⁶⁹ S. A. Majewski,⁶⁹ B. A. Petersen,⁶⁹ L. Wilden,⁶⁹ S. Ahmed,⁷⁰ M. S. Alam,⁷⁰
 R. Bula,⁷⁰ J. A. Ernst,⁷⁰ V. Jain,⁷⁰ B. Pan,⁷⁰ M. A. Saeed,⁷⁰ F. R. Wappler,⁷⁰ S. B. Zain,⁷⁰ W. Bugg,⁷¹
 M. Krishnamurthy,⁷¹ S. M. Spanier,⁷¹ R. Eckmann,⁷² J. L. Ritchie,⁷² A. M. Ruland,⁷² C. J. Schilling,⁷²
 R. F. Schwitters,⁷² J. M. Izen,⁷³ X. C. Lou,⁷³ S. Ye,⁷³ F. Bianchi,⁷⁴ F. Gallo,⁷⁴ D. Gamba,⁷⁴ M. Pelliccioni,⁷⁴
 M. Bomben,⁷⁵ L. Bosisio,⁷⁵ C. Cartaro,⁷⁵ F. Cossutti,⁷⁵ G. Della Ricca,⁷⁵ L. Lanceri,⁷⁵ L. Vitale,⁷⁵ V. Azzolini,⁷⁶
 N. Lopez-March,⁷⁶ F. Martinez-Vidal,⁷⁶ § D. A. Milanes,⁷⁶ A. Oyanguren,⁷⁶ J. Albert,⁷⁷ Sw. Banerjee,⁷⁷
 B. Bhuyan,⁷⁷ K. Hamano,⁷⁷ R. Kowalewski,⁷⁷ I. M. Nugent,⁷⁷ J. M. Roney,⁷⁷ R. J. Sobie,⁷⁷ P. F. Harrison,⁷⁸
 J. Ilic,⁷⁸ T. E. Latham,⁷⁸ G. B. Mohanty,⁷⁸ M. Pappagallo,⁷⁸ ¶ H. R. Band,⁷⁹ X. Chen,⁷⁹ S. Dasu,⁷⁹
 K. T. Flood,⁷⁹ J. J. Hollar,⁷⁹ P. E. Kutter,⁷⁹ Y. Pan,⁷⁹ M. Pierini,⁷⁹ R. Prepost,⁷⁹ S. L. Wu,⁷⁹ and H. Neal⁸⁰

(The BABAR Collaboration)

¹Laboratoire de Physique des Particules, IN2P3/CNRS et Université de Savoie, F-74941 Annecy-Le-Vieux, France

²Universitat de Barcelona, Facultat de Física, Departament ECM, E-08028 Barcelona, Spain

³Università di Bari, Dipartimento di Fisica and INFN, I-70126 Bari, Italy

⁴University of Bergen, Institute of Physics, N-5007 Bergen, Norway

⁵Lawrence Berkeley National Laboratory and University of California, Berkeley, California 94720, USA

⁶University of Birmingham, Birmingham, B15 2TT, United Kingdom

⁷Ruhr Universität Bochum, Institut für Experimentalphysik 1, D-44780 Bochum, Germany

⁸University of Bristol, Bristol BS8 1TL, United Kingdom

⁹University of British Columbia, Vancouver, British Columbia, Canada V6T 1Z1

¹⁰Brunel University, Uxbridge, Middlesex UB8 3PH, United Kingdom

¹¹Budker Institute of Nuclear Physics, Novosibirsk 630090, Russia

¹²University of California at Irvine, Irvine, California 92697, USA

¹³University of California at Los Angeles, Los Angeles, California 90024, USA

¹⁴University of California at Riverside, Riverside, California 92521, USA

¹⁵University of California at San Diego, La Jolla, California 92093, USA

¹⁶University of California at Santa Barbara, Santa Barbara, California 93106, USA

¹⁷University of California at Santa Cruz, Institute for Particle Physics, Santa Cruz, California 95064, USA

¹⁸California Institute of Technology, Pasadena, California 91125, USA

¹⁹University of Cincinnati, Cincinnati, Ohio 45221, USA

²⁰University of Colorado, Boulder, Colorado 80309, USA

²¹Colorado State University, Fort Collins, Colorado 80523, USA

²²Universität Dortmund, Institut für Physik, D-44221 Dortmund, Germany

²³Technische Universität Dresden, Institut für Kern- und Teilchenphysik, D-01062 Dresden, Germany

²⁴Laboratoire Leprince-Ringuet, CNRS/IN2P3, Ecole Polytechnique, F-91128 Palaiseau, France

- ²⁵University of Edinburgh, Edinburgh EH9 3JZ, United Kingdom
- ²⁶Università di Ferrara, Dipartimento di Fisica and INFN, I-44100 Ferrara, Italy
- ²⁷Laboratori Nazionali di Frascati dell'INFN, I-00044 Frascati, Italy
- ²⁸Università di Genova, Dipartimento di Fisica and INFN, I-16146 Genova, Italy
- ²⁹Harvard University, Cambridge, Massachusetts 02138, USA
- ³⁰Universität Heidelberg, Physikalisches Institut, Philosophenweg 12, D-69120 Heidelberg, Germany
- ³¹Imperial College London, London, SW7 2AZ, United Kingdom
- ³²University of Iowa, Iowa City, Iowa 52242, USA
- ³³Iowa State University, Ames, Iowa 50011-3160, USA
- ³⁴Johns Hopkins University, Baltimore, Maryland 21218, USA
- ³⁵Universität Karlsruhe, Institut für Experimentelle Kernphysik, D-76021 Karlsruhe, Germany
- ³⁶Laboratoire de l'Accélérateur Linéaire, IN2P3/CNRS et Université Paris-Sud 11, Centre Scientifique d'Orsay, B. P. 34, F-91898 ORSAY Cedex, France
- ³⁷Lawrence Livermore National Laboratory, Livermore, California 94550, USA
- ³⁸University of Liverpool, Liverpool L69 7ZE, United Kingdom
- ³⁹Queen Mary, University of London, E1 4NS, United Kingdom
- ⁴⁰University of London, Royal Holloway and Bedford New College, Egham, Surrey TW20 0EX, United Kingdom
- ⁴¹University of Louisville, Louisville, Kentucky 40292, USA
- ⁴²University of Manchester, Manchester M13 9PL, United Kingdom
- ⁴³University of Maryland, College Park, Maryland 20742, USA
- ⁴⁴University of Massachusetts, Amherst, Massachusetts 01003, USA
- ⁴⁵Massachusetts Institute of Technology, Laboratory for Nuclear Science, Cambridge, Massachusetts 02139, USA
- ⁴⁶McGill University, Montréal, Québec, Canada H3A 2T8
- ⁴⁷Università di Milano, Dipartimento di Fisica and INFN, I-20133 Milano, Italy
- ⁴⁸University of Mississippi, University, Mississippi 38677, USA
- ⁴⁹Université de Montréal, Physique des Particules, Montréal, Québec, Canada H3C 3J7
- ⁵⁰Mount Holyoke College, South Hadley, Massachusetts 01075, USA
- ⁵¹Università di Napoli Federico II, Dipartimento di Scienze Fisiche and INFN, I-80126, Napoli, Italy
- ⁵²NIKHEF, National Institute for Nuclear Physics and High Energy Physics, NL-1009 DB Amsterdam, The Netherlands
- ⁵³University of Notre Dame, Notre Dame, Indiana 46556, USA
- ⁵⁴Ohio State University, Columbus, Ohio 43210, USA
- ⁵⁵University of Oregon, Eugene, Oregon 97403, USA
- ⁵⁶Università di Padova, Dipartimento di Fisica and INFN, I-35131 Padova, Italy
- ⁵⁷Laboratoire de Physique Nucléaire et de Hautes Energies, IN2P3/CNRS, Université Pierre et Marie Curie-Paris6, Université Denis Diderot-Paris7, F-75252 Paris, France
- ⁵⁸University of Pennsylvania, Philadelphia, Pennsylvania 19104, USA
- ⁵⁹Università di Perugia, Dipartimento di Fisica and INFN, I-06100 Perugia, Italy
- ⁶⁰Università di Pisa, Dipartimento di Fisica, Scuola Normale Superiore and INFN, I-56127 Pisa, Italy
- ⁶¹Prairie View A&M University, Prairie View, Texas 77446, USA
- ⁶²Princeton University, Princeton, New Jersey 08544, USA
- ⁶³Università di Roma La Sapienza, Dipartimento di Fisica and INFN, I-00185 Roma, Italy
- ⁶⁴Universität Rostock, D-18051 Rostock, Germany
- ⁶⁵Rutherford Appleton Laboratory, Chilton, Didcot, Oxon, OX11 0QX, United Kingdom
- ⁶⁶DSM/Dapnia, CEA/Saclay, F-91191 Gif-sur-Yvette, France
- ⁶⁷University of South Carolina, Columbia, South Carolina 29208, USA
- ⁶⁸Stanford Linear Accelerator Center, Stanford, California 94309, USA
- ⁶⁹Stanford University, Stanford, California 94305-4060, USA
- ⁷⁰State University of New York, Albany, New York 12222, USA
- ⁷¹University of Tennessee, Knoxville, Tennessee 37996, USA
- ⁷²University of Texas at Austin, Austin, Texas 78712, USA
- ⁷³University of Texas at Dallas, Richardson, Texas 75083, USA
- ⁷⁴Università di Torino, Dipartimento di Fisica Sperimentale and INFN, I-10125 Torino, Italy
- ⁷⁵Università di Trieste, Dipartimento di Fisica and INFN, I-34127 Trieste, Italy
- ⁷⁶IFIC, Universitat de Valencia-CSIC, E-46071 Valencia, Spain
- ⁷⁷University of Victoria, Victoria, British Columbia, Canada V8W 3P6
- ⁷⁸Department of Physics, University of Warwick, Coventry CV4 7AL, United Kingdom
- ⁷⁹University of Wisconsin, Madison, Wisconsin 53706, USA
- ⁸⁰Yale University, New Haven, Connecticut 06511, USA

With a sample of 232×10^6 $\Upsilon(4S) \rightarrow B\bar{B}$ events collected with the BABAR detector, we study the decays of B mesons to $p\bar{p}h$ final states, where $h = \pi^+, K_s^0, K^{*0}$ or K^{*+} . We report evidence for the $B^0 \rightarrow p\bar{p}K^{*0}$ decay, with a branching fraction $(1.5 \pm 0.5(\text{stat}) \pm 0.4(\text{syst})) \times 10^{-6}$, and for the $B^+ \rightarrow \eta_c K^{*+}$ decay, with the branching fraction of $\mathcal{B}(B^+ \rightarrow \eta_c K^{*+}) \times \mathcal{B}(\eta_c \rightarrow p\bar{p}) =$

$(1.57_{-0.45}^{+0.56}(\text{stat})_{-0.36}^{+0.46}(\text{syst})) \times 10^{-6}$, and provide improved measurements of the branching fractions of the other modes of this type. We also report the measurements of the charge asymmetry consistent with zero in the $B^+ \rightarrow p\bar{p}\pi^+$, $B^0 \rightarrow p\bar{p}K^{*0}$ and $B^+ \rightarrow p\bar{p}K^{*+}$ modes. No evidence is found for the pentaquark candidate Θ^+ in the mass range 1.52 to 1.55 GeV/ c^2 , decaying into pK_S^0 , or the glueball candidate $f_J(2220)$ in the mass range $2.2 < m_{p\bar{p}} < 2.4$ GeV/ c^2 , and branching fraction limits are established for both at the 10^{-7} level.

PACS numbers: 13.25.Hw, 12.15.Hh, 11.30.Er

I. INTRODUCTION

This paper reports measurements of the branching fractions of the baryonic three-body decays $B \rightarrow p\bar{p}h$ where $h = \pi^+$, K_S^0 , \bar{K}^{*0} , or K^{*+} and their resonant substructures. This work is a continuation of our study of the $B^+ \rightarrow p\bar{p}K^+$ decay reported in Ref. [1]. Observations of these decays were reported earlier in Ref. [2], except for the channel $B^0 \rightarrow p\bar{p}K^{*0}$, for which only an upper limit was obtained.

These channels are interesting for the dynamical information in the distribution of the three final-state particles and for the possible presence of exotic intermediate states, such as a pentaquark candidate $\Theta^+(1540)$ in the $m_{pK_S^0}$ spectrum [3] or an $f_J(2220)$ glueball candidate in the $m_{p\bar{p}}$ spectrum [4].

The quark diagrams of the three-body baryonic B decays are described in detail in Ref. [5]; only the dominant contributions are described below. In particular, the $B^+ \rightarrow p\bar{p}\pi^+$ decay proceeds mainly through external and internal W -emission ‘‘tree’’ processes, while in the decay $B^0 \rightarrow p\bar{p}K^{0(*)}$ a virtual loop ‘‘penguin’’ process $b \rightarrow sg$ is expected to be dominant. The $B^+ \rightarrow p\bar{p}K^{+(*)}$ decay receives contributions from both the penguin and the doubly Cabibbo-Kobayashi-Maskawa-suppressed external W -emission tree processes.

An important feature of $B \rightarrow p\bar{p}h$ decays is an enhancement at low $p\bar{p}$ masses reported in Ref. [2], similar to that seen in several other baryonic decays of B mesons [6] and J/ψ [7]. This enhancement might reflect short-range correlations between p and \bar{p} in a fragmentation chain [5, 8]. Alternatively, it could be a feature of a quasi-two-body decay in which the $p\bar{p}$ system is produced through an intermediate resonance [4], in particular the $X(1835)$ state recently observed by BES [9]. Rosner [10] proposed distinguishing between the two mechanisms by studying the distribution of events in the Dalitz plot. As in the case of the resonance, p and \bar{p} are produced independent from a hadron, then the distributions m_{ph} and

$m_{\bar{p}h}$ should be identical.

Ten experimental groups reported narrow enhancements near 1.54 GeV/ c^2 in the invariant-mass spectra for nK^+ and pK^0 [11]. The minimal quark content of a state that decays strongly to nK^+ is $dduu\bar{s}$: therefore, these mass peaks were interpreted as a possible pentaquark state, called $\Theta(1540)^+$. On the other hand, a number of experiments that observe strange baryons with mass similar to that of the $\Theta(1540)^+$ [e.g., $\Lambda(1520) \rightarrow pK^-$] see no evidence for the $\Theta(1540)^+$ [12, 13]. As suggested in Ref. [3] we search for a pentaquark baryon candidate Θ^+ , in the $m_{pK_S^0}$ mass distribution of $B^0 \rightarrow p\bar{p}K^0$ decays.

A narrow state $f_J(2220)$ with a width of 23 MeV was reported in the $K\bar{K}$ spectrum by the MARK III experiment [14] and later seen in K^+K^- , $K^0\bar{K}^0$, $\pi^+\pi^-$ and $p\bar{p}$ by the BES [15] experiment. However, its non-observation in quite a few $p\bar{p}$ annihilation modes, in particular in $p\bar{p} \rightarrow f_J(2220) \rightarrow K\bar{K}$ [16], has led to doubts about its existence [17]. One theoretical conjecture [4] suggests a possible presence of the $f_J(2220)$ resonance in baryonic B decays.

Direct CP violation is observable as an asymmetry in yields between a decay and its CP conjugate when at least two contributing amplitudes carry different weak and strong phases. Following the observation of the direct CP violation in $B^0 \rightarrow K^+\pi^-$ [18] transitions and its non-observation in $B^+ \rightarrow K^+\pi^0$ [19], it is interesting to study the charge asymmetry in the $B \rightarrow p\bar{p}h$ system. Three-body baryonic B decays to $p\bar{p}h$ occur through two different mechanisms (penguin and tree), which carry different weak phases and, in general, different strong phases. Although negligible direct CP violation asymmetry is measured in the $B^+ \rightarrow p\bar{p}K^+$ mode [1, 2], recent theoretical calculations predict a significant asymmetry in the $B^+ \rightarrow p\bar{p}K^{*+}$ mode [20].

We use events with the same final state particles to isolate the decay $B^0 \rightarrow \Lambda_c^+\bar{p}$, $\Lambda_c^+ \rightarrow pK^{0(*)}$ and decays $B \rightarrow X_{c\bar{c}}h$, for $X_{c\bar{c}} = \eta_c$ and J/ψ , with a subsequent decay to $p\bar{p}$. Charge-conjugate reactions are included implicitly throughout the paper.

In Sec. II, we describe the *BABAR* detector. In Secs. III, IV, and V we discuss the reconstruction of the B -meson candidates, the branching fraction (B.F.) extraction and the systematic uncertainties, respectively. In Sec. VI we present our results on the $B \rightarrow p\bar{p}h$, $B \rightarrow X_{c\bar{c}}h$ and $B^0 \rightarrow \Lambda_c^+\bar{p}$ branching fraction measurements, charge-asymmetry measurements, and searches for $\Theta(1540)^+$ pentaquark and $f_J(2220)$ glueball states. We discuss the $B \rightarrow p\bar{p}h$ decay dynamics and summarize

*Deceased

[†]Also with Università di Perugia, Dipartimento di Fisica, Perugia, Italy

[‡]Also with Università della Basilicata, Potenza, Italy

[§]Also with Universitat de Barcelona, Facultat de Física, Departament ECM, E-08028 Barcelona, Spain

[¶]Also with IPPP, Physics Department, Durham University, Durham DH1 3LE, United Kingdom

in Secs. VII and VIII, respectively.

II. BABAR DETECTOR AND DATA SAMPLE

This measurement is performed with a data sample of $232 \times 10^6 \Upsilon(4S) \rightarrow B\bar{B}$ decays corresponding to an integrated luminosity of 210 fb^{-1} , collected at the $\Upsilon(4S)$ resonance (“on-resonance”) with the BABAR detector at the PEP-II e^+e^- storage ring. An additional 21 fb^{-1} of data (“off-resonance”), collected about 40 MeV below the resonance, is used to study the backgrounds from light-quark and $c\bar{c}$ production. The BABAR detector is described in detail elsewhere [21]. Charged-particle trajectories are measured by a five-layer silicon vertex tracker (SVT) and a 40-layer drift chamber (DCH), both operating in a 1.5-T solenoidal magnetic field. A Cherenkov radiation detector (DIRC) is used for charged-particle identification. The CsI(Tl) electromagnetic calorimeter detects photon and electron showers. The BABAR detector Monte Carlo simulation based on GEANT4 [22] is used to optimize selection criteria and to determine selection efficiencies.

III. B MESON RECONSTRUCTION

The B^+ and B^0 decays are reconstructed in the following modes: $B^+ \rightarrow p\bar{p}\pi^+$, $B^0 \rightarrow p\bar{p}K^{*0}$, $B^0 \rightarrow p\bar{p}K_s^0$ and $B^+ \rightarrow p\bar{p}K^{*+}$. Charged tracks not coming from K_s^0 must originate from the interaction point, have transverse momentum greater than $0.1 \text{ GeV}/c$, and at least twelve DCH hits. Charged pions, kaons and protons are identified by the average energy loss (dE/dx) in the tracking devices and by the pattern of Cherenkov photons in the DIRC. The $K_s^0 \rightarrow \pi^+\pi^-$ candidates are required to have a two-pion invariant mass within $8 \text{ MeV}/c^2$ of the nominal K_s^0 mass [12] and a cosine of the angle between the line connecting the B and K_s^0 decay vertices and the K_s^0 momentum greater than 0.999 in the laboratory frame. K^{*+} candidates are reconstructed in the $K^{*+} \rightarrow K_s^0\pi^+$ decay channel, and K^{*0} candidates are reconstructed in the $K^{*0} \rightarrow K^+\pi^-$ mode. Candidates whose mass is within $80 \text{ MeV}/c^2$ of the nominal K^* mass [12] are selected as K^* candidates, and the ones with mass $160 - 240 \text{ MeV}/c^2$ away from the K^* mass are chosen as the K^* sideband sample. The three daughters in the B decay are fit constraining their paths to a common vertex. To suppress background, we impose a cut requiring a probability greater than 10^{-4} on the each of the K_s^0 and the B candidates’ vertices.

Two kinematic constraints of B -meson pair-production at the $\Upsilon(4S)$ are used to characterize the B candidates: the beam-energy-substituted mass $m_{ES} = [(E_{cm}^2/2 + \mathbf{p}_0 \cdot \mathbf{p}_B)^2/E_0^2 - \mathbf{p}_B^2]^{1/2}$ and the energy difference $\Delta E = E_B^* - E_{cm}/2$, where E_{cm} is the total center-of-mass energy, E_B^* is the center-of-mass energy of the B meson candidate (the asterisk denotes the center-of-mass frame throughout the paper), and (E_0, \mathbf{p}_0) is the four-

momentum of the initial state and \mathbf{p}_B is the B momentum in the laboratory frame. For signal B decays the ΔE distribution peaks near zero with a mode-dependent resolution of $11 - 17 \text{ MeV}$, while the m_{ES} distribution peaks near the B meson mass with a mode-dependent resolution of $2.5 - 3.0 \text{ MeV}/c^2$, as determined in Monte Carlo simulation.

We select events with $m_{ES} > 5.22 \text{ GeV}/c^2$ ($5.25 \text{ GeV}/c^2$ for the $B^+ \rightarrow p\bar{p}\pi^+$ mode) and $|\Delta E| < 0.10 \text{ GeV}$ (0.15 GeV for the $B^0 \rightarrow p\bar{p}K_s^0$ mode). We make these selections quite loose since these two variables are used in a maximum likelihood fit to extract the signal yield. Of the candidates passing that loose selection, only one candidate is chosen for each event, selecting the one with the highest B vertex probability, or, if a K_s^0 is present in the decay chain, the highest value of the product of the B and the K_s^0 vertex probabilities. To improve the resulting mass resolutions, after selecting the B candidates we perform a kinematic fit fixing the mass of each B candidate to its known value [12] and its energy to a half of the total center-of-mass energy.

The background is dominated by random combinations of tracks created in $e^+e^- \rightarrow q\bar{q}$ (where q is u, d, s, c quarks) continuum events. These events are collimated along the original quark directions and can be distinguished from more spherical $B\bar{B}$ events. We construct a Fisher discriminant (\mathcal{F}) [23] as a linear combination of the following four event-shape variables:

1. $\cos\theta_{thr}^*$, the cosine of the angle between the thrust axis of the reconstructed B and the beam axis;
2. $\cos\theta_{mom}^*$, the cosine of the angle between the momentum of the reconstructed B and the beam axis;
3. and 4. the zeroth and the second Legendre polynomial momentum moments, L_0 and L_2 . They are defined as follows: $L_0 = \sum_i |\mathbf{p}_i^*|$ and $L_2 = \sum_i |\mathbf{p}_i^*| [(3 \cos^2 \theta_{thrB,i}^* - 1)/2]$, where \mathbf{p}_i^* are the momenta of the tracks and neutral clusters not associated with the B candidate and $\theta_{thrB,i}^*$ is the angle between \mathbf{p}_i^* and the thrust axis of the B candidate.

The coefficients for the Fisher discriminant variables are determined for each of the modes separately by maximizing the separation between the means of the signal and background Fisher discriminant distributions obtained from the signal Monte Carlo samples and the off-resonance data events, respectively.

There is also a background for the three-body decays $B \rightarrow p\bar{p}h$ from B mesons decaying into the same final states as the signal, such as $B \rightarrow X_{c\bar{c}}h$ decays, where $X_{c\bar{c}} = \eta_c, J/\psi, \psi', \chi_{c0}, \chi_{c1}, \chi_{c2}$ decaying to $p\bar{p}$ and the $B^0 \rightarrow \Lambda_c^+\bar{p}$ decay. This background, which is of interest in its own right, is discussed in the next section. Other backgrounds from B decays are negligible.

IV. BRANCHING FRACTION EXTRACTION

We perform an unbinned extended maximum likelihood (ML) fit to extract the signal yields. The variables m_{ES} , ΔE and \mathcal{F} are used as discriminating variables to separate signal from background.

To estimate the contribution from B decays that proceeded through $b \rightarrow c$ transitions leading to the $p\bar{p}h$ final state, such as η_c , $J/\psi \rightarrow p\bar{p}$ and $\Lambda_c^+ \rightarrow pK_s^0/K^{*0}$, the maximum likelihood fit is performed in three distinct regions:

1. The main ‘‘charmonium’’ region which includes the η_c and J/ψ resonances: $2.85 < m_{p\bar{p}} < 3.15 \text{ GeV}/c^2$ (for $h = K^0/K^{*0}/K^{*+}$).
2. The ‘‘charm’’ (Λ_c^+) region delimited by $|m_{ph} - 2.3 \text{ GeV}/c^2| < 0.1 \text{ GeV}/c^2$ where $h = K_s^0/K^{*0}$, and $|m_{p\bar{p}} - 3 \text{ GeV}/c^2| > 0.15 \text{ GeV}/c^2$ (this prevents overlap with the charmonium region). Note that for $h = K_s^0$ both m_{ph} and $m_{\bar{p}h}$ combinations are considered.
3. The ‘‘all-other’’ region. Significant background from slow pions in the $B^+ \rightarrow p\bar{p}\pi^+$ mode leads to a slight difference of the Fisher discriminant shape at low and high $m_{p\bar{p}}$. To reduce the sensitivity to that correlation we perform the fit for this mode in two regions: $m_{p\bar{p}} < 3.6 \text{ GeV}/c^2$ and $m_{p\bar{p}} > 3.6 \text{ GeV}/c^2$.

In the charmonium region, in addition to the three variables described above, the $m_{p\bar{p}}$ variable is used to distinguish between the non-resonant signal and contributions from η_c and J/ψ . In the charm region the corresponding additional variable is m_{ph} .

The data sample is assumed to consist of two components: signal events, including B meson decays to $X_{c\bar{c}}h$ and $\Lambda_c^+\bar{p}$, which have the same final state particles as the signal, and combinatorial background events. The latter are due to random combinations of tracks from both continuum and $B\bar{B}$ events. For the fit in the charmonium region, η_c and J/ψ signal-like components are included in the fit, a Λ_c^+ component corresponding to the overlap of charm and charmonium regions is not included here but its contribution is taken into account in Sec. VIA. For the charm region, a Λ_c^+ component is included in the fit as both signal and background contributions. For the decay $B^+ \rightarrow p\bar{p}\pi^+$, an additional $B^+ \rightarrow p\bar{p}K^+$ component is considered, to account for the $B^+ \rightarrow p\bar{p}K^+$ events present in the fit region because of kaon/pion misidentification. The signal component is split into correctly reconstructed true events and mis-reconstructed events, so-called self-cross-feed (SCF). The SCF events are signal events in which one or more of the tracks from the signal side are lost and a track from the other B decay is included in the reconstruction. The fraction of SCF events is determined with a $B \rightarrow p\bar{p}h$ Monte Carlo sample and varies from 0.5% for the $B^0 \rightarrow p\bar{p}K_s^0$ mode to 5.6% for the $B^+ \rightarrow p\bar{p}K^{*+}$ mode. In the $B^0 \rightarrow p\bar{p}K_s^0$

mode, the SCF signal events are indistinguishable from the combinatorial background and no separate SCF signal component is used in the maximum likelihood fit.

In the maximum likelihood fit, each component is modeled by the product of probability density functions (PDF) of the following variables, which are assumed to be uncorrelated for all components:

- m_{ES} , ΔE , \mathcal{F} and $m_{p\bar{p}}$ in the charmonium region:

$$\mathcal{P}_1^x = \mathcal{P}^x(m_{\text{ES}}, \Delta E, \mathcal{F}, m_{p\bar{p}}) \quad (1)$$

- m_{ES} , ΔE and \mathcal{F} and m_{ph} in the charm region:

$$\mathcal{P}_2^x = \mathcal{P}^x(m_{\text{ES}}, \Delta E, \mathcal{F}, m_{ph}) \quad (2)$$

- m_{ES} , ΔE and \mathcal{F} in the all-other region:

$$\mathcal{P}_3^x = \mathcal{P}^x(m_{\text{ES}}, \Delta E, \mathcal{F}) \quad (3)$$

where x indicates the event source. In the all-other region there are two components: x is either signal (s) or background (b), in the charmonium region there are four components $x = s, \eta_c, J/\psi$ and b ; and in the charm region there are three components $x = s, \Lambda_c^+$ and b .

The likelihood is given by

$$\mathcal{L}_r = e^{-N_r} \prod_{i=1}^{N_r} \sum_x N_r^x \mathcal{P}_r^x, \quad (4)$$

where r corresponds to a fit region, N_r is the total number of events in that region and \sum_x is the sum over all the corresponding fit components in a given region. Then the total number of events in the charmonium region is $N_1 = N_1^s + N^{\eta_c} + N^{J/\psi} + N_1^b$, in the charm region is $N_2 = N_2^s + N^{\Lambda_c^+} + N_2^b$, and in the all-other region is $N_3 = N_3^s + N_3^b$, where N^s , N^{η_c} , $N^{J/\psi}$, $N^{\Lambda_c^+}$ and N^b are the number of non-resonant signal, η_c , J/ψ , Λ_c^+ signal and combinatorial background events, respectively. \mathcal{P}^x is the PDF for a corresponding component x , e.g. \mathcal{P}_r^b is the background PDF for region r . The signal PDF $\mathcal{P}_r^s = \mathcal{P}_r^{\text{true}} + f_{\text{SCF}} \mathcal{P}_r^{\text{SCF}}$ consists of the PDFs of the true and SCF signal events, respectively, with the corresponding fraction of SCF events f_{SCF} as determined from $B \rightarrow p\bar{p}h$ signal Monte Carlo and fixed in the fit.

The parametrization of the $B \rightarrow p\bar{p}h$ true signal, SCF, η_c , J/ψ , Λ_c^+ and combinatorial background components is summarized in Table I.

All parameters in the $B \rightarrow p\bar{p}h$ true and SCF signal PDFs are obtained from corresponding $B \rightarrow p\bar{p}h$ signal Monte Carlo simulations. The $B \rightarrow p\bar{p}h$ signal Monte Carlo events are simulated according to a three-body phase-space decay expectation, which has been shown in Refs. [1, 2] not to reproduce the data. In order to improve the parametrization for the $B \rightarrow p\bar{p}h$ signal PDFs the signal Monte Carlo events are re-weighted according to the $m_{p\bar{p}}$ distributions from $B^+ \rightarrow p\bar{p}K^+$ given in Refs. [1, 2].

TABLE I: The PDF parametrization of $B \rightarrow p\bar{p}h$ signal, self-cross-feed (SCF), η_c , J/ψ , A_c^+ and combinatorial background contributions. We use the following notation: ‘‘BifGauss’’ for a Bifurcated Gaussian, ‘‘G’’ for a Gaussian (2×G are two Gaussian distributions with common mean), ‘‘Voigtian’’ for a convolution of a Breit-Wigner distribution and a sum of Gaussian distributions with common mean, ‘‘ARGUS’’ for a threshold function [24], ‘‘norm’’ for normalization and ‘‘ratio’’ is a ratio of the normalizations of a linear to a Gaussian contributions. The parameters floated for each of the functions are specified in the brackets.

Component	m_{ES}	ΔE	\mathcal{F}	$m_{p\bar{p}}$	m_{ph}
$B^0 \rightarrow p\bar{p}K_s^0$					
signal	BifGauss (mean)	G+G (narrow mean)	G+G	constant (norm)	constant (norm)
J/ψ	same as signal	same as signal	same as signal	2×G (narrow σ)	–
η_c	same as signal	same as signal	same as signal	2×Voigtian	–
A_c^+	same as signal	same as signal	same as signal	–	2×G
combinatorial	ARGUS (slope)	linear (all)	G+G (means)	linear	linear+2×G (ratio)
$B^+ \rightarrow p\bar{p}K^{*+}$					
signal	BifGauss (mean)	G+G (narrow mean)	G+G	constant (norm)	–
J/ψ	same as signal	same as signal	same as signal	2×G (narrow σ)	–
η_c	same as signal	same as signal	same as signal	2×Voigtian	–
SCF	ARGUS	linear	G+G	constant	–
combinatorial	ARGUS (slope)	linear (all)	G (all)	linear	–
$B^0 \rightarrow p\bar{p}K^{*0}$					
signal	BifGauss (mean)	G+G (narrow mean)	G+G	constant (norm)	constant (norm)
J/ψ	same as signal	same as signal	same as signal	2×G (narrow σ)	–
η_c	same as signal	same as signal	same as signal	2×Voigtian	–
A_c^+	same as signal	same as signal	same as signal	–	2×G
SCF	ARGUS+G	quadratic	G+G	constant	–
combinatorial	ARGUS (slope)	linear (all)	G (all)	linear	linear+2×G (ratio)
$B^+ \rightarrow p\bar{p}\pi^+$					
signal	BifGauss (mean)	G+G (narrow mean)	G+G	–	–
SCF	ARGUS	linear	G+G	–	–
$p\bar{p}K^+$	BifGauss	G+G	G+G	–	–
$p\bar{p}K^+$ SCF	ARGUS	linear	G+G	–	–
combinatorial	ARGUS (slope)	linear (all)	G+G (all)	–	–

The m_{ES} , ΔE , and \mathcal{F} PDFs for the η_c , J/ψ and A_c^+ contributions are taken to be the same as the corresponding PDFs for the $B \rightarrow p\bar{p}h$ signal. The known masses of the J/ψ and A_c^+ and the known mass and width of the η_c are used in the fits. All the other parameters that are not floated are fixed to the values obtained from the corresponding Monte Carlo simulation.

All the parameters for the $B^+ \rightarrow p\bar{p}K^+$ background events in the $B^+ \rightarrow p\bar{p}\pi^+$ mode are fixed in the fit to the values obtained from the $B^+ \rightarrow p\bar{p}K^+$ Monte Carlo events re-weighted as described above as well as the expected amount of the charmonium events with $p\bar{p}K^+$ final states.

For the combinatorial background events all the parameters fixed in the fit are obtained from the on- $\mathcal{T}(4S)$ resonance data m_{ES} sideband ($m_{ES} < 5.26 \text{ GeV}/c^2$).

The parametrization of the signal and combinatorial background PDFs does not vary with the fit region.

The remaining floating parameters of the PDFs are determined by a maximum likelihood fit to the data. The fit uses the kinematic variables described above but is independent of the location of the event in the Dalitz plot. This fit not only determines the various parameters of

the PDFs, but also the number of signal and background events, and the covariance matrix for these event numbers.

Once the maximum likelihood fit provides the best estimate of the PDF parameters, we use a weighting technique [25] to measure the branching fraction and reconstruct efficiency-corrected mass distributions. This method allows us to take into account the dependence of the efficiency on the position of a candidate in the Dalitz plot. We assume that the distributions in the variables m_{ES} , ΔE , and \mathcal{F} are uncorrelated with the location in the Dalitz plot.

The event-dependent weight to be signal, \mathcal{W}_s^j (also known as the *sWeight* in the *sPlots* method [25]), is computed from the PDFs:

$$\mathcal{W}_s^j = \frac{\sum_x \mathbf{V}_r(s, x) \mathcal{P}_r^{x,j}}{\sum_x N_r \mathcal{P}_r^{x,j}}, \quad (5)$$

where $\mathcal{P}_r^{x,j}$ is the value of the PDF for the component x ($x = \text{signal, background, charmonium-signal, charmonium-}\eta_c$, etc.) in the event j for the fit region r (as defined in Equations 1-3), and $\mathbf{V}_r(s, x)$ is the co-

variance between the number of signal events N_r^s and the number of events for the component x , N_r^x , in the fit region r defined by:

$$\mathbf{V}_r(s, x)^{-1} = \frac{\partial^2(-\ln \mathcal{L})}{\partial N_r^s \partial N_r^x} = \sum_{j=1}^{N_r} \frac{\mathcal{P}_r^{s,j} \mathcal{P}_r^{x,j}}{(\sum_x N_r^x \mathcal{P}_r^{x,j})^2}. \quad (6)$$

The sum of \mathcal{W}_s^j over all events j is just $N^s = N_1^s + N_2^s + N_3^s$, while the sum of \mathcal{W}_s^j over all events in a small area in phase space gives, in the limit of high statistics, the correct distribution of the signal in that area while preserving the total signal yield. These weights (\mathcal{W}_s^j) allow optimal discrimination between signal-like and background-like events [25] and serve as a tool to reconstruct the resulting signal distributions.

The resulting branching fraction is then calculated as follows:

$$\mathcal{B} = \sum_{j=1}^N \frac{\mathcal{W}_s^j}{N_{B\bar{B}} \cdot \varepsilon_j \cdot \mathcal{B}_{\text{sub}}}, \quad (7)$$

where the sum is over all events j , $N_{B\bar{B}}$ is the total number of $B\bar{B}$ pairs, \mathcal{B}_{sub} is the product of the branching fractions in the sub-decays and ε_j is the reconstruction efficiency of the event j . The reconstruction efficiency depends on the position of the candidate on the Dalitz plane and is obtained from the corresponding signal Monte Carlo simulations. The statistical error on the branching fraction is given by

$$\frac{\Delta \mathcal{B}}{\mathcal{B}} = \frac{\sqrt{\sum_{j=1}^N \frac{(\mathcal{W}_s^j)^2}{\varepsilon_j^2}}}{\sum_{j=1}^N \frac{\mathcal{W}_s^j}{\varepsilon_j}}. \quad (8)$$

V. SYSTEMATIC ERRORS

The contributions to the systematic errors on the measured branching fractions and charge asymmetries are summarized in Tables II and III.

The $Y(4S)$ is assumed to decay equally to $B^0\bar{B}^0$ and B^+B^- mesons. Incomplete knowledge of the luminosity and cross-section leads to a 1.1% uncertainty in all branching fraction measurements. Charged-tracking, particle-identification (PID) and K_S^0 reconstruction studies of the data lead to small corrections applied to each track in these simulations. Limitations of statistics and purity in these data-Monte Carlo comparisons lead to residual systematic uncertainties. Limitation of Monte Carlo statistics employed in each analysis contributes a small uncertainty. The effects of binning on the efficiency are estimated by studying the variation in the resulting signal yield due to changes in the chosen bin size.

A large control sample of $B \rightarrow J/\psi(e^+e^-, \mu^+\mu^-)h$ is studied separately in data and Monte Carlo simulations to understand uncertainties arising from the choice of vertexing cuts and from the parametrization of the PDFs

for ΔE , m_{ES} and \mathcal{F} (this uncertainty is labeled ‘‘Pre-Selection’’ in Table II).

The uncertainty due to possible correlation between the fit variables is estimated by performing fits to a number of Monte Carlo experiments that consist of fully simulated signal events embedded in parametrized background simulations. This so-called ‘‘Fit Bias’’ uncertainty in Table II) is on the order of a few percent.

Where the Monte Carlo values are used to fix signal shape parameters in a fit, we obtain the uncertainty on the signal yield due to a change in each of the PDF parameters by doing a number of toy Monte Carlo experiments with parametrized signal and background distributions. In each a fit is performed with the original value of the PDF parameter and the value shifted by its uncertainty, which is obtained from the $B \rightarrow p\bar{p}h$ signal Monte Carlo simulation. The resulting uncertainties are added together in quadrature, taking into account the correlation between the PDF parameters, to obtain the total error for each PDF. The procedure is repeated using the correlation matrices between the variables to obtain the total error for each fit component, which is then added in quadrature to give the total error on PDF parametrization.

In a similar fashion, different fit ranges for charmonium and charm regions are employed and the resulting variation of the fit yields is taken as a systematic error.

The potential correlation of the fit variables with their location on the Dalitz plot would slightly violate the main principle of the *sPlot* method. To reduce the sensitivity to that correlation the fit is performed in one, two and four $m_{p\bar{p}}$ regions for all the modes. The resulting variation of the branching fraction is taken as a systematic error. Note that we constrained the $B^+ \rightarrow p\bar{p}K^{*+}$ fit to make the signal component non-negative (in the charmonium region), which results in additional systematic error on the fit region. All the uncertainties above are summed in quadrature to give the ‘‘Fit Region’’ error in Table II).

Branching fraction uncertainties [12] on $\mathcal{B}(B^+ \rightarrow Xh) \times \mathcal{B}(X \rightarrow p\bar{p})$, where $X = \chi_{c[0,1,2]}, \psi'$ and $h = K_S^0, K^{*0}$ or K^{*+} , and on the sub-branching fractions of K^0 and K^* , which affect the $B \rightarrow p\bar{p}h$ branching fraction measurements, are given in the ‘‘ B Bkg / B.F. errors’’ line in Table II.

For modes that contain K^* mesons, the non-resonant $K\pi$ background is obtained by performing a maximum likelihood fit and extracting the branching fraction in the K^* sideband region. The non-resonant $K\pi$ contributions to the branching fraction values, based on the K^* sideband data, for the the $B^+ \rightarrow p\bar{p}K^{*+}$ and $B^0 \rightarrow p\bar{p}K^{*0}$ modes are $(0.34 \pm 0.74) \times 10^{-6}$ and $(0.23 \pm 0.30) \times 10^{-6}$, correspondingly. The K^* -sideband signal yields for $J/\psi K^{*0}$ and $J/\psi K^{*+}$ are $11.5^{+4.3}_{-3.5}$ and $1.2^{+1.7}_{-0.9}$ events; for $\eta_c K^{*0}$ and $\eta_c K^{*+}$ are 0 ± 5.7 and $1.8^{+2.9}_{-2.0}$ events; for the $B \rightarrow \Lambda_c^+ \bar{p}$ in the $B^0 \rightarrow p\bar{p}K^{*0}$ mode $4.5^{+3.6}_{-2.7}$ events. As no significant non-resonant $K\pi$

TABLE II: Systematic errors (in percent) and efficiency corrections for all modes. The efficiency correction is a weight applied event-by-event to signal efficiency to account for residual differences between signal Monte Carlo and data.

Error Source	$p\bar{p}K^0$	$p\bar{p}K^{*+}$	$p\bar{p}K^{*0}$	$p\bar{p}\pi^+$	$\eta_c K^0$	$\eta_c K^{*+}$	$\eta_c K^{*0}$	$\bar{p}\Lambda_c^+(pK^0)$	$\bar{p}\Lambda_c^+(pK^{*0})$	Θ^+
$B\bar{B}$ counting	1.1	1.1	1.1	1.1	1.1	1.1	1.1	1.1	1.1	1.1
PID efficiency	1.2	1.6	3.4	2.1	1.2	1.6	2.9	1.6	3.6	-5.8/+6.6
Track reconstruction	1.6	2.4	3.6	2.4	1.6	2.4	3.2	1.6	3.2	1.6
K_S^0 reconstruction	2.8	2.9	n/a	n/a	1.1	1.2	n/a	2.1	n/a	1.6
Monte Carlo Statistics	2.0	-3.4/+4.4	2.5	2.6	0.3	1.3	0.8	1.2	1.0	0.3
Dalitz plot binning	2.1	3.5	1.4	2.0	n/a	n/a	n/a	n/a	n/a	n/a
Pre-selection	0.5	0.8	0.4	0.3	0.5	0.8	0.4	0.5	0.4	0.5
Fit Bias	5.0	3.0	3.6	1.1	3.4	3.4	1.5	20.0	11.0	n/a
PDF Parametrization	3.0	-3.7/+3.2	-1.9/+2.2	6.2	1.1	-3.3/+3.8	3.0	1.3	0.6	n/a
Fit Region	5.7	17.0	6.5	13.0	5.0	1.8	3.0	5.0	3.4	n/a
B Bkg / B.F. errors	1.0	0.8	2.9	0.8	n/a	n/a	n/a	n/a	n/a	n/a
Non-resonant $K\pi$	n/a	15.4	25.2	n/a	n/a	-21.9/+22.7	15.5	n/a	-42.7/+46.9	n/a
Total(%)	9.5	24.4	27.1	15.2	6.7	-22.8/+23.6	16.8	21.0	-44.5/+48.6	-6.3/+7.1
Pre-selection correction	0.976	0.967	0.968	0.983	0.976	0.967	0.968	0.969	0.968	0.976
K_S^0 correction	0.981	0.980	n/a	n/a	0.972	0.966	n/a	0.976	n/a	n/a

TABLE III: Systematic errors for the charge asymmetry measurements.

Error	$p\bar{p}K^{*+}$	$p\bar{p}K^{*0}$	$p\bar{p}\pi^+$	$\eta_c K^{*+}$	$\eta_c K^{*0}$	$J/\psi K^{*+}$	$J/\psi K^{*0}$
Track Reconstruction	0.002	0.004	0.002	0.002	0.004	0.002	0.004
PID Efficiency	0.003	0.015	0.001	0.001	0.002	0.002	0.001
Monte Carlo Statistics	0.012	0.057	0.021	0.017	0.004	0.002	0.016
Fitting	0.050	0.020	0.040	0.066	0.040	0.018	0.007
Total	0.05	0.06	0.05	0.07	0.04	0.02	0.02

background is seen, we do not perform the sideband subtraction, but rather add these background contributions and their statistical uncertainties in quadrature to give the “Non-resonant $K\pi$ ” systematic uncertainties listed in Table II.

All the uncertainties described above are added in quadrature in the “Total” line in Table II. The final branching fraction value obtained from Eq. 7 is scaled by Pre-selection and “ K_S^0 ” corrections.

VI. RESULTS

A. $B \rightarrow p\bar{p}h$ Branching Fraction Measurements

The event yields from the maximum likelihood fit are presented in Table IV, while Fig. 1 shows projections of the corresponding three-dimensional PDFs on the ΔE and m_{ES} axes. The measured branching fractions calculated from Eq. 7 (scaled by Pre-selection and K_S^0 corrections) are summarized in Table V, where the effective efficiency for the modes observed is calculated accounting for the correct event distribution in the Dalitz plot.

Our fitting method removes all $B \rightarrow \eta_c h$ and $B \rightarrow J/\psi h$ (except in the $B^+ \rightarrow p\bar{p}\pi^+$ mode) contributions and most of the $B^0 \rightarrow \Lambda_c^+ \bar{p}$ contributions. There is

still some remaining $B^0 \rightarrow \Lambda_c^+ \bar{p}$ background contribution from the $B^0 \rightarrow \Lambda_c^+ \bar{p}$ events in the charmonium region. Knowing the relative efficiencies of $B^0 \rightarrow \Lambda_c^+ \bar{p}$ Monte Carlo events inside and outside the charmonium region allows us to calculate the remaining $B^0 \rightarrow \Lambda_c^+ \bar{p}$ background contribution to be $(0.04 \pm 0.02) \times 10^{-6}$ and $(0.06 \pm 0.03) \times 10^{-6}$ for the $B^0 \rightarrow p\bar{p}K^0$ and the $B^0 \rightarrow p\bar{p}K^{*0}$ modes, respectively.

The remaining unknown background comes from the $B \rightarrow \chi_{c0} h$ events. It is possible to estimate the $B^0 \rightarrow \chi_{c0} K^0$ branching fraction using the corresponding $B^+ \rightarrow \chi_{c0} K^+$ branching fraction measurement. Because of isospin symmetry one would expect ratios of the charged and neutral B mesons decaying into χ_{c0} and χ_{c1} to be equal. Thus we estimate [12]: $\mathcal{B}(B^0 \rightarrow \chi_{c0} K^0) \approx \mathcal{B}(B^+ \rightarrow \chi_{c0} K^+) \frac{\mathcal{B}(B^0 \rightarrow \chi_{c1} K^0)}{\mathcal{B}(B^+ \rightarrow \chi_{c1} K^+)} = (1.6^{+0.5}_{-0.4}) \times 10^{-4} \times \frac{3.9 \pm 0.4}{5.3 \pm 0.7} = (0.12 \pm 0.04) \times 10^{-3}$. This number needs to be multiplied by the $\mathcal{B}(\chi_{c0} \rightarrow p\bar{p}) = (0.22 \pm 0.03) \times 10^{-3}$ and results in the expected contributions to the branching fraction from this mode of $(0.026 \pm 0.009) \times 10^{-6}$. The resulting contribution to the absolute systematic error on the B background is 0.009×10^{-6} . The contribution from the $B \rightarrow \chi_{c0} h$ events is ignored for other modes [26].

From Ref. [12] we estimate the contribution of $B^+ \rightarrow J/\psi \pi^+$ to the $B^+ \rightarrow p\bar{p}\pi^+$ mode and the remaining char-

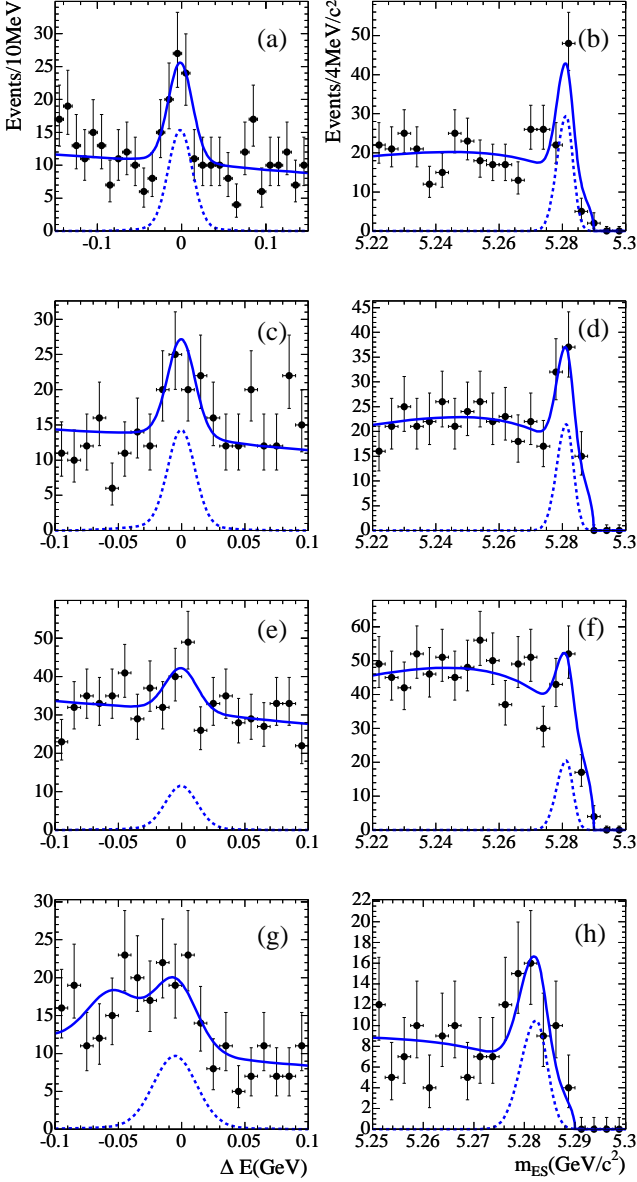


FIG. 1: Distributions (points with error bars) of ΔE and m_{ES} for data candidates passing loose selection in the $B^0 \rightarrow p\bar{p}K^0$ (a)-(b), $B^+ \rightarrow p\bar{p}K^{*+}$ (c)-(d), $B^0 \rightarrow p\bar{p}K^{*0}$ (e)-(f), $B^+ \rightarrow p\bar{p}\pi^+$ (g)-(h) modes. The superimposed solid curves represent the projections on the three-dimensional-fit PDFs on the respective axis, and the dashed line is the fitted signal contribution. Note that the excess of events on the left of the signal peak in (g) corresponds to the $B^+ \rightarrow p\bar{p}K^+$ final states, where K^+ is mis-identified as π^+ . The following loose selection is applied: (a) $m_{ES} > 5.275 \text{ GeV}/c^2$ and $\mathcal{F} > 0.2$; (b) $|\Delta E| < 0.02 \text{ GeV}/c^2$ and $\mathcal{F} > 0.2$; (c) $m_{ES} > 5.275 \text{ GeV}/c^2$ and $\mathcal{F} > 0.2$; (d) $|\Delta E| < 0.02 \text{ GeV}/c^2$ and $\mathcal{F} > 0.2$; (e) $m_{ES} > 5.275 \text{ GeV}/c^2$ and $\mathcal{F} > 0.6$; (f) $|\Delta E| < 0.015 \text{ GeV}/c^2$ and $\mathcal{F} > 0.6$; (g) $m_{ES} > 5.275 \text{ GeV}/c^2$ and $\mathcal{F} > 1.5$; (h) $|\Delta E| < 0.015 \text{ GeV}/c^2$ and $\mathcal{F} > 1.5$.

TABLE IV: Summary of the resulting yields from the maximum likelihood fit for all modes.

Region	charmonium	charm	All-Other	Total
$B^0 \rightarrow p\bar{p}K_S^0$ mode.				
Signal	17_{-8}^{+9}	3_{-3}^{+4}	70_{-11}^{+12}	90_{-14}^{+16}
η_c	23_{-7}^{+8}			23_{-7}^{+8}
J/ψ	53_{-7}^{+8}			53_{-7}^{+8}
A_c^+		$6.8_{-2.8}^{+3.6}$		$6.8_{-2.8}^{+3.6}$
Background	1152 ± 34	1096 ± 33	14769 ± 122	17017 ± 131
$B^+ \rightarrow p\bar{p}K^{*+}$ mode.				
Signal	0 ± 9		52_{-10}^{+11}	52 ± 14
η_c	$12.3_{-3.6}^{+4.4}$			$12.3_{-3.6}^{+4.4}$
J/ψ	34 ± 6			34 ± 6
Background	766 ± 28		10063 ± 101	10829 ± 105
$B^0 \rightarrow p\bar{p}K^{*0}$ mode.				
Signal	8_{-8}^{+10}	4_{-4}^{+6}	50_{-13}^{+14}	63_{-16}^{+18}
η_c	37_{-9}^{+10}			37_{-9}^{+10}
J/ψ	106 ± 11			106 ± 11
A_c^+		$12.3_{-4.1}^{+4.9}$		$12.3_{-4.1}^{+4.9}$
Background	2207 ± 47	1971 ± 45	26312 ± 163	30490 ± 176
$B^+ \rightarrow p\bar{p}\pi^+$ mode.				
Signal			185 ± 28	185 ± 28
$p\bar{p}K^+$			157 ± 30	157 ± 30
Background			90438 ± 305	90438 ± 305

monium contributions ($B \rightarrow \chi_{c1}h$ and $B \rightarrow \psi(2S)h$) for all the other modes. Since only an upper limit exists for the branching fraction of the $B \rightarrow \chi_{c2}h$ mode, it is not subtracted but taken as a one sided contribution to systematic uncertainty. The total expected B background contribution is quoted in the line “ B bkgr. B.F.”

The line “Final B.F.” in Table V summarizes the values of the charmless and charmoniumless $B \rightarrow p\bar{p}h$ branching fractions after B background subtraction.

We report the first evidence for the $B^0 \rightarrow p\bar{p}K^{*0}$ decay with a significance of 3.2σ (including systematic uncertainties). The statistical significance σ throughout the paper is taken as $\sqrt{-2\ln(\mathcal{L}(0)/\mathcal{L}_{max})}$, where $\mathcal{L}(0)$ is the likelihood of the fit assuming zero signal events and \mathcal{L}_{max} is the likelihood obtained in the full fit. For the $B^0 \rightarrow p\bar{p}K^{*0}$ decay the $\mathcal{L}(0)$ is taken to be not at zero signal events, but at the expected number of the B background events as discussed above. To obtain the value of significance including the systematic uncertainties the likelihood function is smeared with a Gaussian distribution which has a width of the corresponding systematic uncertainty.

The measurements of branching fractions for the $B \rightarrow p\bar{p}h$ modes from Ref. [2] and this work are summarized in Table VI and compared to those of the two-body mesonic modes from Refs. [12, 27, 28].

The branching fractions are approximately two times smaller for the $B^+ \rightarrow p\bar{p}K^{*+}$ and the $B^+ \rightarrow p\bar{p}\pi^+$

TABLE V: Summary of the non-charm, non-charmonium $B \rightarrow p\bar{p}h$ branching fraction calculation including B background subtraction. Note that effective efficiency includes the sub-decay branching fractions as well as the correct event distribution in the Dalitz plot.

	$p\bar{p}K^0$	$p\bar{p}K^{*+}$	$p\bar{p}K^{*0}$	$p\bar{p}\pi^+$
Sum of Signal Weights	181±29	52±14	63±17	185±28
Effective Efficiency, %	24.5	4.1	16.0	44.6
B.F. from Eq. 7 (10^{-6})	3.17±0.53	5.45±1.49	1.70±0.45	1.79±0.29
B bkgr. B.F. (10^{-6})	0.22±0.03	0.17±0.04	0.23±0.05	0.10±0.01
Final B.F. (10^{-6})	3.0±0.5±0.3	5.3±1.5±1.3	1.5±0.5±0.4	1.7±0.3±0.3

modes, when compared to the Belle measurements [2], bringing the branching fraction of the $B^+ \rightarrow p\bar{p}K^{*+}$ mode below that of the $B^+ \rightarrow p\bar{p}K^+$ mode and more in line with theoretical predictions [5]. However, the two experiments are in agreement within their errors.

Since the virtual loop ‘‘penguin’’ process $b \rightarrow sg$ preserves isospin we would naively expect the ratio of the rates for $B^+ \rightarrow p\bar{p}K^+$ and $B^0 \rightarrow p\bar{p}K^0$ to be unity as it is in two-body mesonic modes $B \rightarrow \rho^0 h$ and $B \rightarrow \pi^0 h$, but it is closer to two (see Table VI). This could be explained by absence of the external W -emission Feynman tree diagram for the neutral B mode. However, if this tree diagram were important, we would expect a much larger rate for $B^+ \rightarrow p\bar{p}\pi^+$ than for $B^+ \rightarrow p\bar{p}K^+$, in contradiction with the data. The $B^+ \rightarrow p\bar{p}K^{*+}$ branching fraction is also larger (by a factor of three) than that of $B^0 \rightarrow p\bar{p}K^{*0}$ similar to the pattern suggested by the data for decays to $\rho^0 K^*$ and $\pi^0 K^*$. The $B \rightarrow p\bar{p}K^*$ modes are consistently smaller than the $B \rightarrow p\bar{p}K$ modes in both the charged and neutral cases. This seems to be the case for the $B \rightarrow \pi^0 h$ modes as well, but not for the $B \rightarrow \rho^0 h$ modes. The $B^+ \rightarrow p\bar{p}\pi^+$ branching fraction is lower than that of the $B^+ \rightarrow p\bar{p}K^+$ mode as expected because the $b \rightarrow u$ transition at tree level is suppressed compared to the $b \rightarrow s$ penguin. This is similar to what is observed in the $B \rightarrow \pi^0 h$ modes but contrary to what is observed in $B \rightarrow \rho^0 h$.

Overall, the theoretical calculations of the baryonic B decays are not very certain and the current measurements of the branching fractions of all four $B \rightarrow p\bar{p}K$ modes are a further challenge to our understanding.

B. $B \rightarrow (J/\psi, \eta_c)h$ Branching Fraction Measurements

Using the η_c and J/ψ yields from Table IV we obtain the branching fractions shown in Table VII. The values obtained are consistent with current world averages [12]. We also report the first evidence for the $B^+ \rightarrow \eta_c K^{*+}$ decay, with a significance of 3.2σ (including systematic uncertainties). A sample of the maximum likelihood fit result for the charmonium region is shown in Fig. 2.

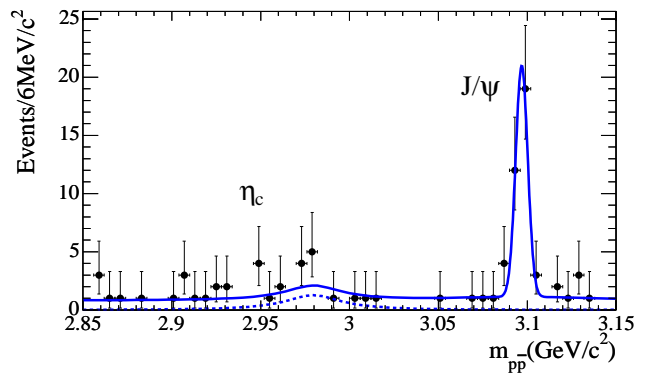


FIG. 2: The results of the maximum likelihood fit for $m_{ES} > 5.27 \text{ GeV}/c^2$ and $|\Delta E| < 0.03 \text{ GeV}$ for the $B^+ \rightarrow p\bar{p}K^{*+}$ mode. The solid line represents results of the fit and the dashed line shows the η_c yield.

C. $B^0 \rightarrow \Lambda_c^+ \bar{p}$ Branching Fraction Measurement

From the $B \rightarrow \Lambda_c^+ \bar{p}$ fit yields in the $B^0 \rightarrow p\bar{p}K_s^0$ and $B^+ \rightarrow p\bar{p}K^{*+}$ modes given in Table IV we obtain the branching fractions shown in Table VIII. Averaging results for both modes and adding the errors in quadrature (except the systematic error on B -counting), we obtain the branching fraction $\mathcal{B}(B^0 \rightarrow \Lambda_c^+ \bar{p}) = (21.0_{-5.5}^{+6.7}(\text{stat})_{-6.2}^{+6.7}(\text{syst})_{-1.7}^{+2.1}(\Lambda_c^+ \text{ B.F.})_{-4.3}^{+7.4}(\mathcal{B}_{\Lambda_c^+ \rightarrow pK\pi})) \times 10^{-6}$. This measurement is consistent with the current value of $\mathcal{B}(B^0 \rightarrow \Lambda_c^+ \bar{p}) = (21.9_{-4.9}^{+5.6} \pm 3.2 \pm 5.7) \times 10^{-6}$ based on a single measurement by Belle [29].

D. $B \rightarrow p\bar{p}h$ Charge Asymmetry Measurements

The CP -violating charge asymmetry is defined as $A_{ch} = (N_{\bar{B}} - N_B)/(N_{\bar{B}} + N_B)$, where N_B and $N_{\bar{B}}$ are the event yields in each of the categories of interest. The events yields are obtained from the maximum likelihood fit described in the Sec. IV, by integrating over the resulting signal event weights for each of the two charge categories separately. The resulting yields for all the modes (except $B^0 \rightarrow p\bar{p}K^0$, which does not have information on the flavor of B meson) are summarized in Table IX. The measurements for the current modes are consistent with

TABLE VI: Summary of the experimental values for the branching fractions ($\times 10^{-6}$) of $B \rightarrow p\bar{p}h$ and their comparison to two-body mesonic modes. The values for the two-body mesonic modes are taken from Ref. [12] unless otherwise noted. The values in **bold** are those presented in the current work.

h	Belle $B \rightarrow p\bar{p}h$ [2]	BABAR $B \rightarrow p\bar{p}h$	$B \rightarrow \pi^0 h$	$B \rightarrow \rho^0 h$
K^+	$6.0 \pm 0.3 \pm 0.4$	$6.7 \pm 0.5 \pm 0.4$ [1]	12.1 ± 0.8	$5.0^{+0.7}_{-0.8}$
K^0	$2.08^{+0.52}_{-0.38} \pm 0.24$	$3.0 \pm 0.5 \pm 0.3$	11.5 ± 1.0	$5.4^{+0.9}_{-1.0}$ [27]
K^{*+}	$10.3^{+3.6}_{-2.8} \pm 1.3$	$5.3 \pm 1.5 \pm 1.3$	6.9 ± 2.4	11.0 ± 4.0
K^{*0}	$< 7.6, 90\% \text{ CL}$	$1.5 \pm 0.5 \pm 0.4$	$< 3.5, 90\% \text{ CL}$	5.6 ± 1.6 [28]
π^+	$1.68^{+0.19}_{-0.17} \pm 0.12$	$1.7 \pm 0.3 \pm 0.3$	5.5 ± 0.6	8.7 ± 1.1

TABLE VII: Summary of the resulting branching fractions for the η_c and J/ψ modes (the order of the uncertainties is as follows: statistical, systematic, due to partial branching fraction correction where appropriate). The following values of branching fractions are used $\mathcal{B}(\eta_c \rightarrow p\bar{p}) = (1.3 \pm 0.4) \times 10^{-3}$ and $\mathcal{B}(J/\psi \rightarrow p\bar{p}) = (2.12 \pm 0.10) \times 10^{-3}$ [12].

$p\bar{p}X$	Efficiency	$\mathcal{B}(B \rightarrow \eta_c(p\bar{p})X) (10^{-6})$		$\mathcal{B}(B \rightarrow \eta_c X) (10^{-3})$	
Mode	%	Measured	PDG [12]	Measured	PDG [12]
$p\bar{p}K^0$	36.3	$0.83^{+0.28}_{-0.26} \pm 0.05$	1.56 ± 0.71	$0.64^{+0.22}_{-0.20} \pm 0.04^{+0.28}_{-0.15}$	1.2 ± 0.4
$p\bar{p}K^{*0}$	23.7	$1.03^{+0.27}_{-0.24} \pm 0.17$	2.08 ± 1.11	$0.80^{+0.21}_{-0.19} \pm 0.13^{+0.35}_{-0.19}$	1.6 ± 0.7
$p\bar{p}K^{*+}$	15.7	$1.57^{+0.56+0.45}_{-0.46-0.36}$	-	$1.21^{+0.43+0.34+0.54}_{-0.35-0.28-0.28}$	-
Mode	Efficiency	$\mathcal{B}(B \rightarrow J/\psi(p\bar{p})X) (10^{-6})$		$\mathcal{B}(B \rightarrow J/\psi X) (10^{-3})$	
$p\bar{p}K^0$	37.1	$1.87^{+0.28}_{-0.26} \pm 0.07$	1.80 ± 0.08	$0.88^{+0.13}_{-0.12} \pm 0.03 \pm 0.04$	0.85 ± 0.04
$p\bar{p}K^{*0}$	25.0	$2.82^{+0.30+0.36}_{-0.28-0.35}$	2.78 ± 0.20	$1.33^{+0.14}_{-0.13} \pm 0.17^{+0.07}_{-0.06}$	1.31 ± 0.07
$p\bar{p}K^{*+}$	17.8	$3.78^{+0.72+0.28}_{-0.64-0.23}$	2.86 ± 0.25	$1.78^{+0.34+0.13+0.09}_{-0.30-0.11-0.08}$	1.35 ± 0.10

zero within less than three standard deviations.

E. $\mathcal{B}(B^0 \rightarrow \Theta(1540)^+ \bar{p})$ Upper Limit Calculation

As suggested in Ref. [3], we search for a pentaquark baryon candidate, Θ^+ , in the $m_{pK_S^0}$ mass distribution of $B^0 \rightarrow p\bar{p}K^0$ decays. If Θ^+ decays strongly, there are only two possible decays modes: nK^+ and pK^0 . For this measurement we assume $\mathcal{B}(\Theta \rightarrow pK_S^0) = 25\%$. From dedicated signal Monte Carlo we determine that the Θ^+ invariant mass resolution is represented by a sum of two Gaussian functions with common mean. The resolution of the main (secondary) Gaussian is $0.95(2.32) \text{ MeV}/c^2$ and the wider Gaussian contributes 19% of the total. The overall resolution, defined as the full width at half maximum of the resolution function divided by 2.4, is $1 \text{ MeV}/c^2$ at the Θ^+ mass of $1.54 \text{ GeV}/c^2$. The Θ^+ pentaquark signal efficiency is $30.8 \pm 0.1\%$. No events are observed in the Θ^+ region of $1.52 < m_{pK_S^0} < 1.55 \text{ GeV}/c^2$ (see Ref. [30] for details). A Bayesian approach is used to calculate the upper limit of 0.20×10^{-6} at 90% confidence level, assuming Poisson-distributed events in the absence of background, including a multiplicative systematic error of 7.1%. This value is consistent with and improves on the upper limit from the Belle Collaboration $\mathcal{B}(B^0 \rightarrow \Theta(1540)^+ \bar{p}) < 0.92 \times 10^{-6}$ [2].

F. Search for glueball $f_J(2220)$ in $B \rightarrow p\bar{p}h$ decays

We search for the narrow state $f_J(2220)$ by scanning through the $2.2 < m_{p\bar{p}} < 2.4 \text{ GeV}/c^2$ region with a $30 \text{ MeV}/c^2$ mass window in the final states $p\bar{p}K^0$ and $p\bar{p}K^*$. This procedure is described in detail in Ref. [30]. The largest upper limits at 90% confidence level, including multiplicative systematic uncertainties of 2.7(4.3 and 4.8)%, on the product of branching fractions are found to be $\mathcal{B}(B \rightarrow f_J(2220)h) \times \mathcal{B}(f_J(2220) \rightarrow p\bar{p}) < 4.5(7.7 \text{ and } 1.5) \times 10^{-7}$ for $h = K^0(K^{*+} \text{ and } K^{*0})$, respectively, assuming the $f_J(2220)$ width is less than 30 MeV .

VII. STUDY OF THE $B \rightarrow p\bar{p}h$ DECAY DYNAMICS

For decay dynamics studies, the maximum likelihood fit is performed using three variables (m_{ES} , ΔE and Fisher discriminant) simultaneously over the whole Dalitz plot, with the exception of the $p\bar{p}\pi^+$ mode where we perform the fit in two regions: $m_{p\bar{p}} < 3.6 \text{ GeV}/c^2$ and $m_{p\bar{p}} > 3.6 \text{ GeV}/c^2$.

The resulting background-subtracted efficiency-corrected Dalitz plots for all the modes are shown in Fig. 3. The main features of the Dalitz plots are expected to be the charmonium resonances (with $J/\psi \rightarrow p\bar{p}$ and $\eta_c \rightarrow p\bar{p}$ bands most prominent), potential Λ_c^+ bands

TABLE VIII: Summary of the resulting branching fractions for $B^0 \rightarrow \Lambda_c^+ \bar{p}$ (the order of the uncertainties is as follows: statistical, systematic, the uncertainty in the ratio of the $\mathcal{B}(\Lambda_c^+ \rightarrow pK^0/K^{*0})$ to the $\mathcal{B}(\Lambda_c^+ \rightarrow pK\pi)$ [12] and the uncertainty in the $\mathcal{B}(\Lambda_c^+ \rightarrow pK\pi)$ value [12]). Note that efficiency does not include the sub-decay branching fractions.

Λ_c^+ decay	Efficiency, %	$\mathcal{B}(\Lambda_c^+ \rightarrow pX)(10^{-3})$ [12]	$\mathcal{B}(B^0 \rightarrow \Lambda_c^+ \bar{p})(10^{-6})$	statistical significance
pK^0	25.4	23 ± 6	$15.1^{+8.0}_{-6.2} \pm 3.2^{+1.4+5.3}_{-1.2-3.2}$	3.4
pK^{*0}	19.7	16 ± 5	$26.9^{+10.7+13.0+4.0+9.4}_{-9.0-12.0-3.1-5.5}$	4.3

TABLE IX: Summary of the asymmetry study: event yields for each of the categories of interest and the charge asymmetry. We observe no statistically significant CP asymmetries.

Events Type	$N_{\bar{B}}$	N_B	A_{ch}
$B^0 \rightarrow p\bar{p}K^{*0}$ mode.			
Signal	35 ± 6	28 ± 5	$0.11 \pm 0.13 \pm 0.06$
η_c	23 ± 5	13 ± 4	$0.28 \pm 0.16 \pm 0.04$
J/ψ	63 ± 8	43 ± 7	$0.19 \pm 0.10 \pm 0.02$
Background	15050 ± 123	15443 ± 125	-0.013 ± 0.006
$B^+ \rightarrow p\bar{p}K^{*+}$ mode.			
Signal	34 ± 6	18 ± 4	$0.32 \pm 0.13 \pm 0.05$
η_c	7 ± 3	5 ± 2	$0.20 \pm 0.28 \pm 0.07$
J/ψ	18 ± 4	16 ± 4	$0.07 \pm 0.17 \pm 0.02$
Background	5453 ± 74	5377 ± 73	0.007 ± 0.010
$B^+ \rightarrow p\bar{p}\pi^+$ mode.			
Signal	97 ± 10	89 ± 9	$0.04 \pm 0.07 \pm 0.04$
Background	45434 ± 213	44968 ± 212	0.005 ± 0.003

in $B^0 \rightarrow p\bar{p}K^0$ and $B^0 \rightarrow p\bar{p}K^{*0}$ modes, as well as the low $p\bar{p}$ mass enhancements. Figure 4 shows the corresponding background Dalitz distributions. The combinatorial background events favor the edges of the Dalitz plot, as they are dominated by the inclusion of random low-momentum tracks.

Background-subtracted efficiency-corrected $m_{p\bar{p}}$ distributions are shown in Fig. 5 and are summarized in Table X. Although the $m_{p\bar{p}}$ enhancement at low mass is quite prominent in the $B^0 \rightarrow p\bar{p}K^0$ and $B^+ \rightarrow p\bar{p}\pi^+$ modes, in the case of the $B^0 \rightarrow p\bar{p}K^{*0}$ and $B^+ \rightarrow p\bar{p}K^{*+}$ modes the statistics are too limited to draw a definite conclusion. Note that the shapes of the enhancement in $B^0 \rightarrow p\bar{p}K^0$ and $B^+ \rightarrow p\bar{p}K^{*+}$ [1] are similar within the statistics of the measurements, in agreement with the theoretical predictions [5].

To shed light on the nature of this enhancement [10], its uniformity on the Dalitz plot has been tested. The Dalitz plot is divided along the diagonal $m_{ph} = m_{\bar{p}h}$ line and each of the two halves is projected onto the nearer axis. If the Dalitz plot is symmetric we expect the number of events in both projections to be the same. The corresponding background-subtracted efficiency-corrected distributions for the signal events in all the modes are shown in Fig. 6. No asymmetry is expected to be introduced from variations in $\varepsilon_{m_{p\bar{p}}}$ which is charge-symmetric and slowly varying with $m_{p\bar{p}}$.

In the case of $B^0 \rightarrow p\bar{p}K^0$, there is no information on the flavor of the B meson and thus this study cannot be

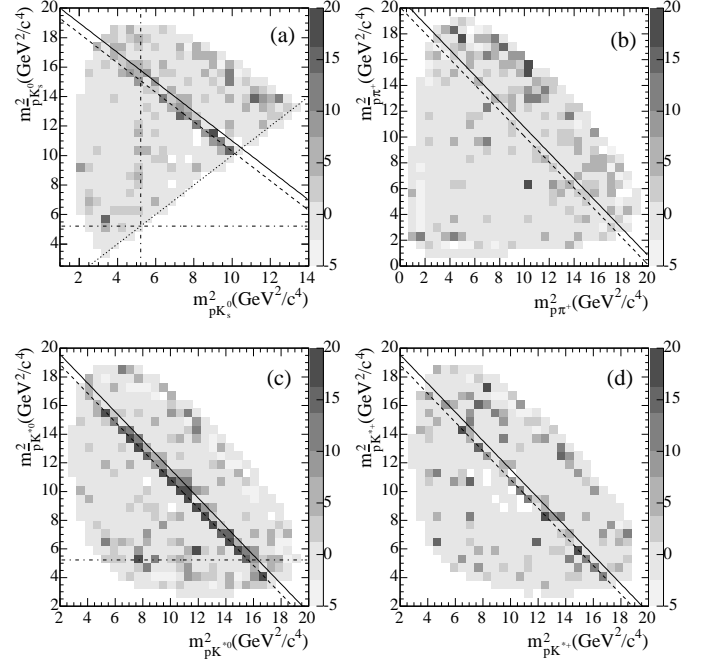


FIG. 3: Dalitz plots for signal in the (a) $B^0 \rightarrow p\bar{p}K^0$, (b) $B^+ \rightarrow p\bar{p}\pi^+$, (c) $B^0 \rightarrow p\bar{p}K^{*0}$ and (d) $B^+ \rightarrow p\bar{p}K^{*+}$ modes obtained using the weighting technique described in Ref. [25]. The positions of the following resonances are shown: η_c in solid, J/ψ in dashed and Λ_c in dot-dashed lines. Note, that because of fluctuations and uncertainties, the signal rate in many bins is negative. The white areas correspond to regions with no entries.

performed. For the $B^+ \rightarrow p\bar{p}K^{*+}$ mode there seems to be no difference between the two halves within the available statistics. In the $B^0 \rightarrow p\bar{p}K^{*0}$ mode there might be a marginal excess at low m_{ph} , which could be caused by the presence of the standard baryon resonances (such as Λ_c^+), while in the $B^+ \rightarrow p\bar{p}\pi^+$ mode there is a marginal excess of events at high m_{ph} around $3.8 \text{ GeV}/c^2$ in the $m_{p\pi^+}$ half of the Dalitz plot, contrary to the result observed in the $B^+ \rightarrow p\bar{p}K^{*+}$ mode [1]. No quantitative theoretical description of this correlation is available at present. Although the asymmetry in the low $m_{p\bar{p}}$ band shown in [1] disfavors the possibility of the low mass $p\bar{p}$ enhancement originating only from the presence of a resonance below threshold (such as the baryonium candidate at $1835 \text{ MeV}/c^2$ recently seen by BES [9]) the low

TABLE X: Summary of efficiency-corrected, background-subtracted number of events in $m_{p\bar{p}}$ bins for $B^0 \rightarrow p\bar{p}K^0$, $B^+ \rightarrow p\bar{p}\pi^+$, $B^0 \rightarrow p\bar{p}K^{*0}$, and $B^+ \rightarrow p\bar{p}K^{*+}$ modes. Note that contributions from the B decays to charmonium are removed.

$m_{p\bar{p}}$ range (GeV/ c^2)	$B^0 \rightarrow p\bar{p}K^0$	$B^+ \rightarrow p\bar{p}\pi^+$	$B^0 \rightarrow p\bar{p}K^{*0}$	$B^+ \rightarrow p\bar{p}K^{*+}$
1.876 – 2.100	$160 \pm 50 \pm 14$	$96 \pm 30 \pm 9$	$30 \pm 37 \pm 17$	$280 \pm 109 \pm 39$
2.100 – 2.350	$151 \pm 50 \pm 13$	$74 \pm 25 \pm 9$	$7 \pm 34 \pm 16$	$53 \pm 90 \pm 22$
2.350 – 2.600	$80 \pm 40 \pm 7$	$64 \pm 24 \pm 5$	$3 \pm 26 \pm 5$	$213 \pm 95 \pm 18$
2.600 – 2.850	$60 \pm 31 \pm 6$	$83 \pm 27 \pm 8$	$30 \pm 26 \pm 12$	$189 \pm 86 \pm 22$
2.850 – 3.150	$48 \pm 23 \pm 8$	$22 \pm 21 \pm 3$	$32 \pm 38 \pm 5$	$0 \pm 39 \pm 37$
3.150 – 3.400	$-2 \pm 13 \pm 5$	$37 \pm 18 \pm 3$	$32 \pm 21 \pm 6$	$112 \pm 66 \pm 33$
3.400 – 3.600	$3 \pm 22 \pm 8$	$-1 \pm 11 \pm 1$	$64 \pm 27 \pm 8$	$129 \pm 75 \pm 14$
3.600 – 3.900	$13 \pm 27 \pm 5$	$35 \pm 19 \pm 9$	$47 \pm 31 \pm 7$	$84 \pm 80 \pm 17$
3.900 – 4.150	$41 \pm 25 \pm 10$	$11 \pm 9 \pm 1$	$58 \pm 30 \pm 12$	$30 \pm 65 \pm 9$
4.150 – 4.387	$24 \pm 25 \pm 9$	$-2 \pm 7 \pm 1$	$49 \pm 30 \pm 5$	$105 \pm 88 \pm 17$
4.387 – 4.580	$49 \pm 29 \pm 10$	$-11 \pm 4 \pm 3$	$-1 \pm 6 \pm 1$	$0 \pm 11 \pm 3$
4.580 – 4.782	$25 \pm 34 \pm 6$	$0 \pm 12 \pm 17$	n/a	n/a
4.782 – 5.139	n/a	$12 \pm 18 \pm 19$	n/a	n/a

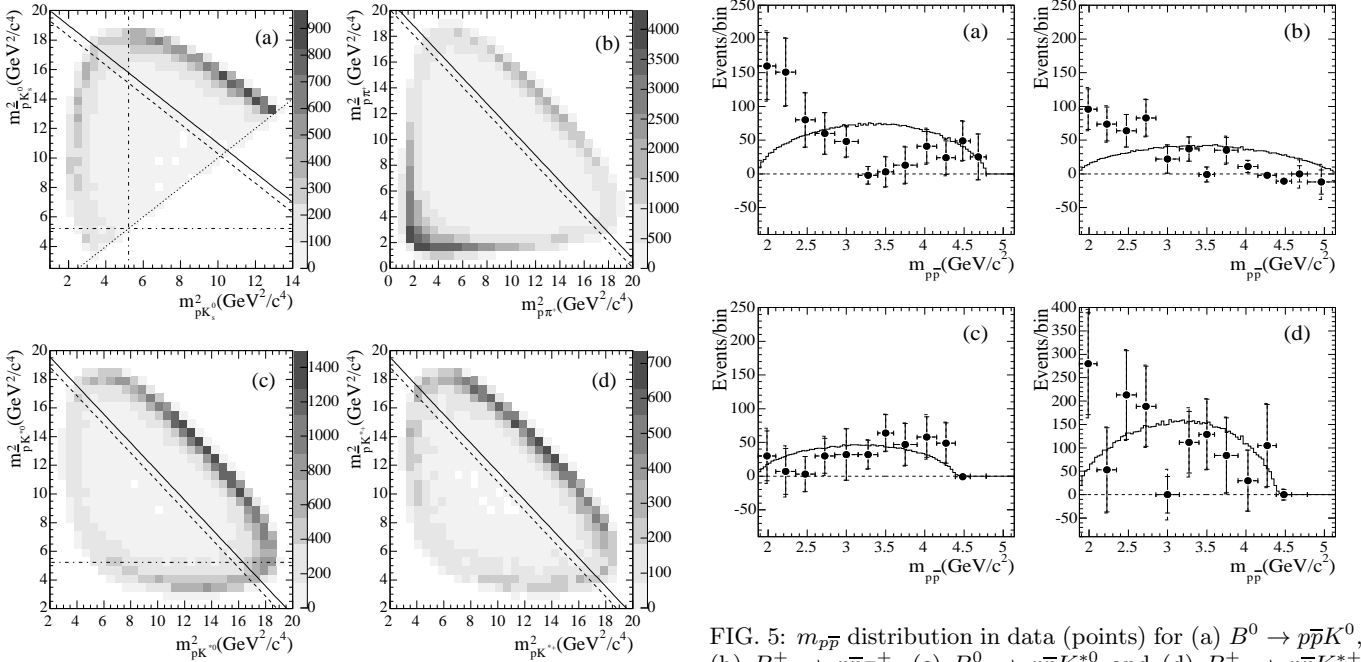


FIG. 4: Dalitz plots for background in the (a) $B^0 \rightarrow p\bar{p}K^0$, (b) $B^+ \rightarrow p\bar{p}\pi^+$, (c) $B^0 \rightarrow p\bar{p}K^{*0}$ and (d) $B^+ \rightarrow p\bar{p}K^{*+}$ modes obtained using the weighting technique described in Ref. [25]. The expected positions of the following resonances are shown: η_c in solid, J/ψ in dashed and Λ_c in dot-dashed lines. The white areas correspond to regions with no entries.

statistics of the current modes does not allow to derive a definite conclusion.

FIG. 5: $m_{p\bar{p}}$ distribution in data (points) for (a) $B^0 \rightarrow p\bar{p}K^0$, (b) $B^+ \rightarrow p\bar{p}\pi^+$, (c) $B^0 \rightarrow p\bar{p}K^{*0}$ and (d) $B^+ \rightarrow p\bar{p}K^{*+}$ modes obtained using the weighting technique described in Ref. [25]. The inner error bars show statistical uncertainty and the outer ones show statistical and systematic uncertainties added in quadrature. The histograms correspond to the relevant three-body phase-space signal Monte Carlo distributions. The dashed line shows zero. The bin size is varying and is specified in Table X. Note that the contribution from the B decays to charmonium is removed.

VIII. CONCLUSIONS

In summary, with 210 fb^{-1} of data, we report evidence for the $B^0 \rightarrow p\bar{p}K^{*0}$ decay with a branching fraction $(1.5 \pm 0.5(\text{stat}) \pm 0.4(\text{syst})) \times 10^{-6}$, and provide improved measurements of branching fractions of the other

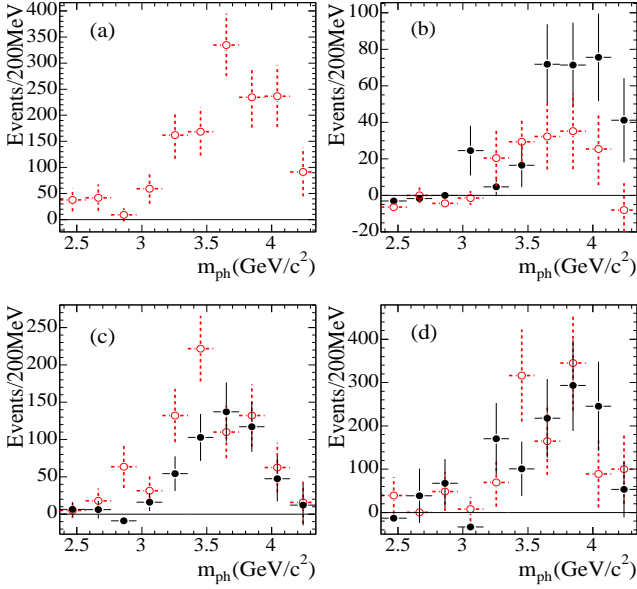


FIG. 6: m_{ph} distribution obtained using the weighting technique described in Ref. [25]: in red (open circles) for $m_{ph} > m_{\bar{p}h}$ and in black (filled circles) for $m_{ph} < m_{\bar{p}h}$ for (a) $B^0 \rightarrow p\bar{p}K^0$, (b) $B^+ \rightarrow p\bar{p}\pi^+$, (c) $B^0 \rightarrow p\bar{p}K^{*0}$ and (d) $B^+ \rightarrow p\bar{p}K^{*+}$. Solid line shows zero. Only statistical error bars are shown.

$B \rightarrow p\bar{p}h$ modes, where $h = \pi^+, K^0$ and K^{*+} . One key observation is that the pattern of decays for $B \rightarrow p\bar{p}h$ differs from that found for $B \rightarrow \pi^0 h$ and $B \rightarrow \rho^0 h$. We also identify decays of the type $B \rightarrow X_{c\bar{c}}h \rightarrow p\bar{p}h$, where $h = K_S^0, K^{*0}$ and K^{*+} , and $X_{c\bar{c}} = \eta_c$ and J/ψ . In particular, we report evidence for the $B^+ \rightarrow \eta_c K^{*+}$ decay with the branching fraction of $\mathcal{B}(B^+ \rightarrow \eta_c K^{*+}) \times \mathcal{B}(\eta_c \rightarrow p\bar{p}) = (1.57^{+0.56}_{-0.45}(\text{stat})^{+0.46}_{-0.36}(\text{syst})) \times 10^{-6}$. We confirm the ear-

lier observation of the $B^0 \rightarrow \Lambda_c^+ \bar{p}$ decay [29] and report measurements of the charge asymmetry consistent with zero in the $B^+ \rightarrow p\bar{p}\pi^+$, $B^0 \rightarrow p\bar{p}K^{*0}$ and $B^+ \rightarrow p\bar{p}K^{*+}$ modes. No evidence is found for the pentaquark candidate Θ^+ in the mass range 1.52 to 1.55 GeV/c^2 , decaying into pK_S^0 , or the glueball candidate $f_J(2220)$ in the mass range $2.2 < m_{p\bar{p}} < 2.4 \text{ GeV}/c^2$, and branching fraction limits are established at the 10^{-7} level.

IX. ACKNOWLEDGMENTS

We are grateful for the extraordinary contributions of our PEP-II colleagues in achieving the excellent luminosity and machine conditions that have made this work possible. The success of this project also relies critically on the expertise and dedication of the computing organizations that support BABAR. The collaborating institutions wish to thank SLAC for its support and the kind hospitality extended to them. This work is supported by the US Department of Energy and National Science Foundation, the Natural Sciences and Engineering Research Council (Canada), the Commissariat à l’Energie Atomique and Institut National de Physique Nucléaire et de Physique des Particules (France), the Bundesministerium für Bildung und Forschung and Deutsche Forschungsgemeinschaft (Germany), the Istituto Nazionale di Fisica Nucleare (Italy), the Foundation for Fundamental Research on Matter (The Netherlands), the Research Council of Norway, the Ministry of Science and Technology of the Russian Federation, Ministerio de Educación y Ciencia (Spain), and the Science and Technology Facilities Council (United Kingdom). Individuals have received support from the Marie-Curie IEF program (European Union) and the A. P. Sloan Foundation.

[1] BABAR Collaboration, B. Aubert *et al.*, Phys. Rev. D **72**, 051101 (2005).
[2] Belle Collaboration, M.Z. Wang *et al.*, Phys. Rev. Lett. **92**, 131801 (2004); Belle Collaboration, M. Z. Wang *et al.*, Phys. Lett. B **617**, 141 (2005); Belle Collaboration, J. T. Wei *et al.*, arXiv:0706.4167 [hep-ex].
[3] J.L. Rosner, Phys. Rev. D **69**, 094014 (2004).
[4] C.K. Chua, W.S. Hou, S.Y. Tsai, Phys. Lett. B **544**, 139 (2002).
[5] H.Y. Cheng, K.C. Yang, Phys. Rev. D **66**, 014020(2002).
[6] Belle Collaboration, M.Z. Wang *et al.*, Phys. Rev. Lett. **90**, 201802 (2003); Belle Collaboration, Y.J. Lee *et al.*, Phys. Rev. Lett. **93**, 211801 (2004); CLEO Collaboration, S. Anderson *et al.*, Phys. Rev. Lett. **86**, 2732 (2001).
[7] BES Collaboration, J.Z. Bai *et al.*, Phys. Rev. Lett. **91**, 022001 (2003).
[8] C.K. Chua, W.S. Hou, S.Y. Tsai, Phys. Rev. D **66**, 054004 (2002); B. Kerbikov, A. Stavinsky, V. Fedotov, Phys. Rev. C **69**, 055205 (2004).

[9] BES Collaboration, M. Ablikim *et al.*, Phys. Rev. Lett. **95**, 262001 (2005).
[10] J.L. Rosner, Phys. Rev. D **68**, 014004 (2003).
[11] LEP Collaboration, T. Nakano *et al.*, Phys. Rev. Lett. **91**, 012002 (2003). SAPHIR Collaboration, J. Barth *et al.*, Phys. Lett. B **572**, 127 (2003). CLAS Collaboration, S. Stepanyan *et al.*, Phys. Rev. Lett. **91**, 252001 (2003). CLAS Collaboration, V. Kubarovsky *et al.*, Phys. Rev. Lett. **92**, 032001 (2004). Erratum; *ibid.*, 049902. DIANA Collaboration, V.V. Barmin *et al.*, Phys. Atom. Nucl. **66**, 1715 (2003). SVD Collaboration, A. Aleev *et al.*, Phys. Atom. Nucl. **68**, 974 (2005) [Yad. Fiz. **68**, 1012 (2005)]. HERMES Collaboration, A. Airapetian *et al.*, Phys. Lett. B **585**, 213 (2004). A.E. Asratyan, A.G. Dolgolenko, and M.A. Kubantsev, Phys. Atom. Nucl. **67**, 682 (2004). COSY-TOF Collaboration, M. Abdalbary *et al.*, Phys. Lett. B **595**, 127 (2004). ZEUS Collaboration, S. Chekanov *et al.*, Phys. Lett. B **591**, 7 (2004).
[12] Particle Data Group, Y.-M. Yao *et al.*, J. Phys. G **33**, 1

- (2006).
- [13] CLAS Collaboration, B. McKinnon *et al.*, Phys. Rev. Lett. **96**, 212001 (2006).
- [14] MARK-III Collaboration, R. M. Baltrusaitis *et al.*, Phys. Rev. Lett. **56**, 107 (1986).
- [15] BES Collaboration, J. Z. Bai *et al.*, Phys. Rev. Lett. **76**, 3502 (1996).
- [16] PS185 Collaboration, P. Barnes *et al.*, Phys. Lett. B **309**, 469 (1993).
- [17] F. E. Close, Int. J. Mod. Phys. A **17**, 3239 (2002).
- [18] BABAR Collaboration, B. Aubert *et al.*, Phys. Rev. Lett. **93** 131801 (2004).
- [19] BABAR Collaboration, B. Aubert *et al.*, Phys. Rev. Lett. **94** 181802 (2005).
- [20] C. Q. Geng, Y. K. Hsiao and J. N. Ng, Phys. Rev. Lett. **98**, 011801 (2007); C. Q. Geng, Y. K. Hsiao and J. N. Ng, Phys. Rev. D **75**, 094013 (2007).
- [21] BABAR Collaboration, B. Aubert *et al.*, Nucl. Instrum. Methods Phys. Res. A **479**, 1 (2002).
- [22] S. Agostinelli *et al.*, Nucl. Instrum. Methods Phys. Res. A **506**, 250 (2003).
- [23] R.A. Fisher, Ann. Eugenics **7**, 179 (1936).
- [24] ARGUS Collaboration, H. Albrecht *et al.*, Phys. Lett. B **241**, 278 (1990).
- [25] M. Pivk and F.R. Le Diberder, Nucl. Instrum. Methods Phys. Res. A **555**, 356 (2005).
- [26] There are 1.70 ± 2.42 , 1.66 ± 1.74 , -0.39 ± 0.06 and -0.86 ± 0.70 events in the χ_{c0} region for each of the modes shown in Table V respectively.
- [27] BABAR Collaboration, B. Aubert *et al.*, Phys. Rev. Lett. **98**, 051803 (2007); Belle Collaboration, A. Garmash *et al.*, Phys. Rev. D **75**, 012006 (2007); we use HFAG averages (<http://www.slac.stanford.edu/xorg/hfag/rare/index.html>).
- [28] BABAR Collaboration, B. Aubert *et al.*, Phys. Rev. Lett. **97**, 201801 (2006).
- [29] Belle Collaboration, N. Gabyshev *et al.*, Phys. Rev. Lett. **90**, 121802 (2003).
- [30] T. Hryn'ova, Ph.D. thesis, Stanford Univ., 2006; SLAC-R-810.